Estimation of pedestrian crowds' properties using commercial tablets and smartphones

Claudio Feliciani[a] and Katsuhiro Nishinari[b,c]

[a]Department of Advanced Interdisciplinary Studies, Graduate School of Engineering, The University of Tokyo, 4-6-1 Komaba, Meguro-ku, Tokyo 153-8904, Japan; [b]Research Center for Advanced Science and Technology, The University of Tokyo, 4-6-1 Komaba, Meguro-ku, Tokyo 153-8904, Japan; [c]Department of Aeronautics and Astronautics, Graduate School of Engineering, The University of Tokyo, 7-3-1 Hongo, Bunkyo-ku, Tokyo 113-8656, Japan

ARTICLE HISTORY
Compiled May 7, 2019

ABSTRACT
In the study, an alternative method to estimate velocity and density in pedestrian crowds is presented. The proposed approach uses angular velocity and acceleration measurements obtained from inertial sensors to judge amount of body motion and therefore estimate walking velocity. Taking into consideration practical aspects, commercial devices (generic tablets and smartphones) are used to measure inertial quantities showing application potentials and but also limitations in regard to accuracy. Several experiments have been performed in increasingly realistic scenarios to assess the suitability of the method for public pedestrian spaces. Results show that estimation for speed and density are very accurate when position and orientation of the devices is known. Estimations are still reliable in more heterogeneous situations employing different devices, with accuracy increasing with the number of pedestrians being surveyed. The proposed approach may help getting a general picture of pedestrian crowds' condition over large areas with greater employment flexibility.

KEYWORDS
Pedestrian traffic; crowd properties; crowd control; inertial sensor; electronic devices

1. Introduction

Urbanization has been a constant trend during the last century and people keep migrating from countryside areas to regional centers, thus contributing to an increase of population in already densely populated cities (Desa, UN 2014). At the same time, transportation costs are decreasing, making it affordable for an increasing number of people to travel over long distances. Transportation network and facilities accommodating passengers are constantly overwhelmed with crowds of people, with the situation being particularly problematic in emerging economies and Asian countries. In addition, large number of people are easily gathered in religious festivals and public events, making the control and management of such crowds a challenging and indispensable task. Failures in crowd planning of events, inability to recognize dangerous

CONTACT Claudio Feliciani. Email: feliciani@jamology.rcast.u-tokyo.ac.jp

situations and act accordingly have resulted in several accidents which took many people's lives over the last decades (Kok, Lim, and Chan 2016; Illiyas et al. 2013).

Already in the ancient empires, city planning and architecture have given importance in creating urban spaces which can effectively use the limited surface available in densely populated areas. In particular, public buildings accommodating a large number of people have been designed to allow a smooth flow of pedestrians moving within them. It is believed that the Coliseum in Rome allowed to evacuate all its 50'000 spectators in just 5 minutes (Helbing and Mukerji 2012), a remarkable performance also compared to modern structures.

Many centuries later the same problems are still present, but technological improvements and an increased interest toward crowd behavior and social psychology have led to a better understanding of pedestrian dynamics, which ultimately led to the definition of different models describing crowd motion (Wąs et al. 2015; Zheng, Zhong, and Liu 2009). Large buildings designated to accommodate huge crowds (such as stadiums or airports) or facilities with important pedestrian traffic (crosswalks, walkways...) are now designed based on established norms (Transportation Research Board 2010; Ministry of Land, Infrastructure, Transport and Tourism – Housing Bureau et al. 2001) and making use of computer simulation to improve pedestrian safety and comfort. Location and number of evacuation exits are carefully chosen based on a variety of factors in which simulation models make an increasingly important role.

However, since human nature is mostly unpredictable, also the most accurate model cannot predict the real behavior in case of evacuations. In addition, also during normal operation there are a number of variables (grouping pattern, age, cultural identity...) which influence crowd motion and behavior (Shimura et al. 2014; Gorrini et al. 2016; Chattaraj, Seyfried, and Chakroborty 2009). Even the most accurate models fail in predicting pedestrian motion when strong heterogeneity arises.

As a consequence, although simulation models and empirical studies are of fundamental importance in the development stage of infrastructures, there is still the need to control crowds during normal operation to ensure safety and comfort. Security personnel usually takes this important role by determining for example which gate/exit should be made available at any given moment and in which direction it is possible to transit. Crowd control is however only efficient when there is enough information available and when enough capacity is dedicated to process this information (Helbing and Mukerji 2012).

Traditionally, surveillance is done by means of cameras which are placed in multiple locations where special attention is required. Control rooms are usually setup to allow operators to grasp a general image of what is happening inside a facility by switching different screens between the multiple cameras available on site. While such an approach is effective under normal conditions, there are also weak points given by the limitations related to the use of cameras. First of all, images are difficult to process and although computer vision is making rapid progresses, lighting condition and crowd density are still an important factor affecting its performances (Johansson et al. 2008; Daamen, Yuan, and Duives 2016). Also, privacy concerns and legal issues sometimes make the use of technologies related with facial recognition and pedestrian counting difficult, thus creating a supplementary hurdle. In addition, in case of evacuation in the presence of fire, it becomes impossible seeing through the smoke. Finally, surveillance cameras are usually fixed and it is not possible to get quick information for locations not covered by them. While static structures usually do not present blind spots, this is not the case during open air or temporary events where setting a large number of cameras may be a difficult task.

Long time extensive data collection, which aims at getting information such as people count in different parts of a city, is also automated and usually dedicated sensors are used. This process is however quite time consuming and expensive, since several sensors need to be located in different areas, making measurement campaign planning a difficult task. Also, accuracy of such sensors is usually quite low (Poapst 2015), limiting the scope of data collection to estimations.

Nowadays, most of the people composing the crowds found in urban areas usually carry electronic devices (smartphones, tablets...) containing both a large number of sensors and a communication interface allowing to quickly transfer large amounts of data over the wireless network. Previous research (details are given in the next section) has shown that inertial sensors can be used to measure pedestrian motion and reconstruct their trajectories (Boltes, Schumann, and Salden 2017; Feliz Alonso, Zalama Casanova, and Gómez García-Bermejo 2009). It has been also shown that inertial sensors allow to detect anomalies from the crowd by evaluating the movement of its members (Mori et al. 2013). Since inertial data are not privacy sensitive and electronic devices can be carried everywhere, using information from the inertial sensors to judge crowd properties would allow to overcome all the limitations found in image related technologies and develop a flexible system to be activated at any location in case of need.

With this said, it should be remarked that most of the research involving the use of inertial (and related) sensors has made use of specialized equipment (Boltes, Schumann, and Salden 2017; Lin, Li, and Lachapelle 2015; Mori et al. 2013; Höflinger, Zhang, and Reindl 2012; Feliz Alonso, Zalama Casanova, and Gómez García-Bermejo 2009) which is largely different from the components found in commercial devices. In a more practical context, sensors from generic commercial devices will have to be used, since it would be unrealistic asking to the general public to carry special sensors for crowd sensing. Part of this task has been covered in the investigations on the human activity recognition (Concone et al. 2017; Su, Tong, and Ji 2014; Lara and Labrador 2013; Nagao, Yanagisawa, and Nishinari 2018), but the main aim of this research branch has been limited in pattern recognition (using quite complex machine learning algorithms), with limited interest on actual measurement. The study presented here aims at investigating the capabilities and limitations related to the use of generic inertial sensors for estimating crowd properties to be employed in data collection for city planning and potentially crowd control.

This paper is organized as follows. At first a short review on different methods used to measure crowds properties is provided. Next, the technical equipment used in this work will be presented, showing strengths and limitations. Later, the proposed method will be tested in different experimental scenarios to judge suitability toward real applications. Finally, conclusions and suggestions for future studies are discussed.

2. Short review on crowd measurement methods

In order to allow a critical comparison of the proposed approach with existing technologies used for crowd measurement, a short review is given below. The aim is to provide the general knowledge necessary to understand strength and limitations of each methods. Readers interested on details are referred to the references provided along the text.

2.1. *Computer vision*

Computer vision is the most common method used to obtain pedestrian trajectories in public spaces. Applications and specific algorithms are numerous and it is beyond the goal of this text to list them all. The review by Kok et al. (Kok, Lim, and Chan 2016) covers many aspects related with computer vision while also discussing important topics in pedestrian dynamics and interested readers are referred to their text for more details.

In general, it is possible to divide computer vision algorithm into two main categories: optical flow and recognition/tracking methods (alternative subdivisions are however possible based on applications). Recently, algorithms based on machine learning and artificial intelligence are also being used (Mohammadi et al. 2017), but the goal is usually clustering and detection of anomalies, with measurement being only a marginal objective.

Junior et al. (Junior, Musse, and Jung 2010) noted that techniques working in non-crowded conditions may fail for packed crowds, with the opposite case being also true. In general, it can be stated that technologies based on the optical flow works well for high density scenarios, while recognition and tracking is more suitable for low density spaces.

2.1.1. Optical flow

Optical flow is a general technique used in different fields and it is commonly employed in fluid-dynamics to detect the motion of fluids. On that purpose, small particles are injected inside a fluid and consequently move following its streamlines. The area to be studied is exposed to strong light exposure by flashing it at constant intervals. Pictures are taken when the flash is on allowing to keep a track of the particles moving inside the fluid. In the case of pedestrians, the head of people already constitute the "particles" immersed inside the crowd and therefore frames from videos can be directly analyzed. More in general, the optical flow technique can be applied to any type of image sequence, but, knowing the size of the particles to be studied help improving the accuracy of the results.

Once a sequence of two images is obtained, an algorithm based on the Fast Fourier Transform (FFT) is used to get the movement of the crowd between both frames (Zhang, Weng, and Yuan 2012). The result is a vector field representing the direction and amount of velocity in each part of the area being studied. Figure 1(a) provides the example of a generic optical flow algorithm applied on a group of pedestrians walking in the same direction. Lanes are clearly recognized by noticing that velocity is particularly high in certain parts of the image.

Since the whole calculation is based on digital images divided into pixels, a calibration is required to convert pixel units into physical units used in the analysis. Calibration can be performed by directly measuring walking speed of pedestrians being analyzed or comparing the motion seen in video with architectural features of known size (the time required to cross a road for example). The optical flow can be applied to any type of image and applications also include detection of speed of vehicles. Under packed conditions, when the whole image is covered by pedestrians or the part occupied by them is clearly defined, optical flow provides an accurate description of the velocities in the different regions (Zhang, Weng, and Yuan 2012). However, for non-crowded scenarios the optical flow may result in some noise created by changes in lighting conditions not related with motion of pedestrians. This is seen for example

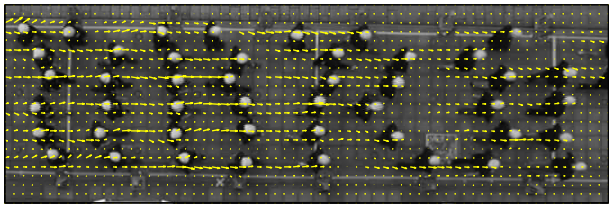

(a) Example of velocity vectors using optical flow.

(b) Pedestrian recognition and tracking using PeTrack (Boltes et al. 2010; Boltes and Seyfried 2013) (trajectories are not complete).

Figure 1. Examples of different computer vision algorithms applied on a group of pedestrians moving in the same direction (from left to right here).

in the upper-left side of Figure 1(a), where velocity vectors are created from a line drawn on the ground.

2.1.2. Recognition and tracking

If density is relatively low and pedestrians are clearly distinguishable one by one, then individual recognition and tracking may be more suitable. The software used to gain trajectories in the controlled experiments presented later is also based on this technique [1].

In contrast to the optical flow approach which provides a general vector field for the whole crowd without distinguishing individuals, the recognition technique allows to obtain single trajectories. The process is divided into two phases: recognition and tracking. The recognition part allows to recognize shapes belonging to individuals. The algorithms used for recognition are more complex than the ones used in the optical flow and they focus on finding typical features of people. Recognition algorithms are typically designed for searching specific characteristics, also depending on the intended applications. If cameras are looking at the crowd from a azimuthal perspective then recognizing the shape of the head may be more efficient. Applications based on security cameras looking frontally to people in very low densities conditions are searching for full body silhouette. Figure 1(b) shows an example of pedestrians detected using PeTrack software (Boltes et al. 2010; Boltes and Seyfried 2013).

Nevertheless, to construct pedestrians' trajectories tracking is necessary, since detection alone cannot link positions found in one frame with the ones corresponding to the previous frame. The tracking algorithm has therefore the aim to link pedestrians and positions and build a unique trajectory composed by the positions occupied from a given pedestrian in all the frames considered. The final result is a set of trajectories each corresponding to a single pedestrian as shown in Figure 1(b).

This technique has the clear advantage of defining accurate positions, thus allowing

[1] Trajectory extraction by having participants wearing colored caps is a well established technique for supervised experiments which started more than ten years ago (Hoogendoorn, Daamen, and Bovy 2003).

(a) Optical camera image.

(b) Distance map using range sensors.

(c) Final result showing position and height of detected pedestrians.

Figure 2. Example showing a practical application of distance sensors to track pedestrians in a real environment (Brscic et al. 2013; Glas et al. 2009). Diagram in (c) is relative to the situation seen in (a), distance map in (b) refers to the same location in a different moment (courtesy of D. Brscic).

complex analysis taking into account pedestrian distance, density and calculations not possible using the optical flow. However, when densities get high, recognizing single individual features inside the crowd may become difficult. Also, when large crowds need to be tracked, the computational requirements rapidly grow, making it difficult to link positions of all individuals between successive frame. Under these conditions one may have to renounce to the accuracy given by trajectory extraction and opt for the more general but reliable approach of the optical flow.

2.2. *Range and distance sensors*

Detection of pedestrians based on images from surveillance cameras has the disadvantage that adequate lighting conditions are required. For instance, detection under darkness is not possible or special cameras are required (e.g. infrared cameras). An alternative method to detect pedestrian motion in public spaces is the use of distance sensors. Distance sensors allow to determine a three-dimensional map including the distance between the sensor and objects lying nearby. If a distance sensor is placed in azimuthal position above a crowd it allows to distinguish standing people from the ground lying at a larger and uniform distance. Also when sensor position is not favorable, pedestrians are clearly distinguished in the distance map as shown in the example of Figure 2(b).

In Figure 2 it is seen that height of detected people can be measured, also allowing to distinguish between adults and children. Once a distance map is generated, then, algorithms similar to the ones for computer vision are used to distinguish single individuals and continuously track their position. One advantage in the use of distance sensors is that privacy sensitive information are not gathered and they can operate under different lighting conditions without any influence on the detection accuracy. However, their range of detection (in terms of surface) is usually limited (typically an area of few meters in width (Corbetta et al. 2016)) and for large scale applications an array of distance sensors is used. The availability of commercial equipment at low cost has seen an increase in the use of this technology and several applications has been reported including single sensors (Seer, Brändle, and Ratti 2014) and arrays connecting several ones (Corbetta et al. 2016; Brscic et al. 2013; Glas et al. 2009). In general, distance sensors are suitable to gain microscopic information, but, when used on a large scale, require important computational power. It is however possible to distribute the different tasks by having some computations performed directly on each

sensor, thus collecting only the summarized information for large scale processing.

2.3. *Alternative approaches*

The methods presented above are mostly focusing on microscopic aspects in the measurement of crowds, with the aim of obtaining velocity and/or density in a building and/or for a festival ground. Computer vision is already a well-established technology and systems based on distance sensors are also finding an increasing number of applications. There are however alternative methods which allow to gain approximate information on different scales ranging from small neighborhood to whole cities or large regions.

For example, WiFi or Bluetooth sensors are used to estimate the travel time between different points on a given route (Abedi et al. 2015). MAC (Media Access Control) scanners are used to detect the presence of electronic devices in the proximity of the sensor. By having several scanners in a specific area it is possible to reconstruct the route of each person by looking for the same MAC address in each scanner's position. In general, only approximate information are gained (such as the average time required to cross a bridge (Abedi et al. 2015)), but in complex environments this approach allows to get a general picture of what is the preferred route and how do the travel time changes during a whole day. The use of WiFi and Bluetooth sensors may become difficult in the presence of many antennas and fixed devices, where considerable noise is created by the different equipments (Abedi et al. 2015).

More in general, we will refer to systems making localization of electronic devices possible using proximity sensing or triangulation techniques as "device proximity sensors". Several technologies are available in this context, making use of different signals to achieve localization accuracy ranging from few centimeters to several meters. The work in (Stojanović and Stojanović 2014) provides an extensive review of different systems categorizing them using criteria similar to the ones introduced here later on. Readers interested in device localization techniques are referred to their work for more details.

An alternative approach to gain information on pedestrian position and travel path is represented by the use of inertial sensors. Inertial sensors are devices capable of measuring changes in velocity and orientation in terms of acceleration and angular velocity. By integrating the signal gained from the measurement of the acceleration it is possible to obtain the velocity, which, by further integration provides the position. If initial position, velocity and orientation are known it is possible to compute the trajectory for one pedestrian by continuously measuring acceleration and angular velocity. In general, devices using inertial sensors also have GPS (Global Positioning System) and compass capabilities, so the initial position can be obtained by one of them or a combination of both. Feliz et al. (Feliz Alonso, Zalama Casanova, and Gómez García-Bermejo 2009) showed that inertial sensors can be efficiently used to obtain pedestrian trajectories also inside buildings without GPS coverage (always provided that initial position is known). In their study, participants had an inertial sensor mounted on their foot registering (three-dimensional) acceleration, angular velocity, magnetic field, air pressure (used to estimate altitude) and GPS position. Despite the good results Feliz et al. also noted that because of the integration steps required to gain position and orientation, errors accumulate over time and particular tricks are required to reduce these effects .

Mori et al. (Mori et al. 2013) also used inertial sensors, but their focus has been on

Table 1. Primary source of information and output generated by data for different types of methods used for crowd monitoring. In case of technologies based on cameras it is assumed that geometry of the considered facility is known and included into the algorithm.

Method / technology	Primary source	Final output	Quantity measured? Velocity	Density
Optical flow	Video image	Velocity vector field	Yes	No
Recognition and tracking	Video image	Position and trajectory	Yes	Yes
Distance sensor	Distance map	Position and trajectory	Yes	Yes
Device proximity sensor	Travel time (position)	Approximate speed	Yes	Yes[a]
GPS	Position	Position and trajectory	Yes	Yes[a]
Specialized sensors fusion	Sensors' measurement	Position and trajectory	Yes	Yes[a]
Generic inertial sensor	**Motion signal**	**Approximate speed**	**Yes**	**No**

[a]Provided that all members of the crowd analyzed are equipped with sensors/devices.

emergency situations and in particular they investigated if it is possible to distinguish between moving behaviors based on the oscillations of the body. In their evacuation experiments an inertial sensor measuring different quantities has been used, but in their analysis only vertical acceleration (in the direction of gravity) has been considered. Mori et al. concluded that by using the maximum of the vertical acceleration of the body it is possible to distinguish between three states typically found in evacuations: stopping, walking or running. The measurement from their sensors were then combined on a large scale approach to detect the outbreak of a disaster.

On very large scales, GPS position is usually used. Although the accuracy of GPS does not allow to use it for building-scale scenarios, the combination with topological information allows to estimate the route taken by people during evacuations from large natural disasters (earthquake, typhoon, flooding...) inside complex metropolitan areas (Sekimoto et al. 2016). In these situations evacuations usually occur outdoor and using public roads, so aggregate information are sufficient and are more important (in particular for policy-makers who have to set priorities on emergency strategies).

Finally, there is a number of sensors working with different principles aimed at counting people passing through a given location. However, as summarized by Poapst (Poapst 2015) such sensors can be quite expensive despite their limited functionality and the counting relative error being in the range of 10–20%. Also, since only counts are obtained it is not possible to estimate speed and density. Nonetheless, such sensors can be useful for long time data collection (several months) and are typically easy to install and use.

2.4. *Summary*

Having discussed the working principles and typical applications of the different technologies we wish now to compare them in a systematic way. Table 1 provides a technical comparison of different approaches, showing the primary source of information on which the analysis is based and the final output after applying the specific algorithms. In addition, considering the goals of this study, capability to measure velocity and density is also given. In Table 1 a distinction is made between the approach combining specialized wearable sensors (gyroscope, accelerometer, barometer, GPS...) and the methodology proposed here which uses generic inertial sensors contained in electronic devices (details on this approach will follow).

Table 2 presents a comparison from a more practical perspective, considering aspects such as computational costs, economical costs, range of application and scalability potential. This table is important to understand what are the expectations

Table 2. Comparison between different types of crowd sensing technology based on several criteria. Computational costs are divided into the sensor level and the requirements for the overall system. Total costs refers only to specialized equipment and/or IT infrastructure; costs of existing generic equipment with possibility to upgrade (surveillance camera, smartphone, tablet...) are excluded. Scalability potential refers to the capability to dynamically change the analyzed region. Range of application considers limitations given for example by smoke or missing illumination.

Method / technology	Accuracy	Computational costs		Total costs	Scalability potential	Range of application
		Sensor	System			
Optical flow	High	Medium	Medium	Medium	Medium	Low
Recognition and tracking	High	High	High	Medium	Low	Low
Distance sensor	High	High	High	High	Low	Low
Device proximity sensor	Low	Low	High	Medium	Medium	Medium
GPS	Low	Low	Medium	Low	High	Medium
Specialized sensors fusion	Medium	Medium	Medium	Medium	High	Medium
Generic inertial sensor	**Medium**	**Low**	**Low**	**Low**	**High**	**High**

in relation to the method presented here and what should be the main aim. As already discussed earlier, technologies based on computer vision are very accurate on the microscopic scale but requires specific hardware and are very expensive in terms of computational costs, especially if trajectories are required. Wearable sensors are more flexible since detection occur where people are and work in all conditions. However, when specialized sensors are required then the range of application would be reduced.

In this study, we wish to develop an approach which allows getting first hand information of crowd condition to enable a first evaluation. Such a system needs to be very flexible and to work in any condition, while also minimizing computational costs to allow a continuous processing of data.

3. Proposed approach and technical description

Accelerometers and gyroscopes are commonly used in electronic devices to interact with users and perform several tasks such as rotate the screen or simulate the motion of vehicles in video games. In this study, we will investigate possible applications of electronic devices (and inertial sensors) for assessing crowd properties such as velocity and density. Before starting with an analysis involving pedestrians, it is however important to test the equipment to evaluate accuracy and eventually limitations. In our previous work we already tested the gyroscope in a bidirectional flow (Feliciani and Nishinari 2016), showing that rotational movements (yawing) measured on pedestrians are in line with indirect calculations based on trajectories. Here, we will use a wider range of sensors and therefore a thorough testing is required.

3.1. *Technical equipment and performances*

In the experiments presented here, Nexus 7 (2013) tablets were chosen due to technical specifications and because of their relative large surface (the tablet is 198.5 mm long, 120 mm wide and 10.5 mm in thickness) and low weight (340 g), which allows to accurately follow body movements while having no (or little) influence on the walking behavior (the authors also tested the tablet on themselves without finding it particularly annoying or interfering normal behavior). An application reading the values generated from the different sensors was installed on each tablet and sensing rate was set at 50 Hz. Because of the differences in clock time between each tablet, a central storage was preferred. Measurements from each tablet were sent over wireless net-

work to a central PC where data were stored [2]. This allowed to obtain the data from each tablet simultaneously (or with a very small delay in the order of milliseconds), independently on the clock time differences between each tablet.

3.1.1. Inertial sensors and measuring principles

Nexus 7 (2013) devices are equipped with a range of sensors (gyroscope, accelerometer, magnetic field, light sensor and GPS), but only few of them were used in our experiments. In particular, we focused on the motion sensor which measures three-dimensional angular velocity and acceleration. It should be mentioned here that there are some differences with the inertial sensors used in the applications described earlier (Feliz et al. and Mori et al. in particular) and the ones contained in Nexus devices. One application of the sensors contained in electronic devices is to determine their orientation mainly for two functions: navigation and screen rotation. In the case of navigation, the compass (based on the magnetic field) plays the most important role, since horizontal orientation is the most relevant to guide users (for example through different roads in a city). To determine the vertical position (and thus rotate the screen if required) the accelerometer is used. The accelerometer needs therefore to determine the direction of gravity by measuring it. As a consequence, while specialized inertial navigation devices record no acceleration at still, accelerometer contained in tablets measures gravity when not moving.

The Android OS (Operating System) on which Nexus devices are running provides however an additional measures called "linear acceleration" which removes the gravity to give only the acceleration relative to the motion of the device [3]. In other words, by using the "linear acceleration" measurement provided from the OS, acceleration is given as zero when the device is at still. However, as we will see later, there are some issues related with this function.

3.1.2. Validation and calibration

Although the inertial sensor contained in tablets is successfully used in a variety of applications, it is not, strictly speaking, a certified scientific instrument. We need therefore to check the accuracy and the precision in the measurement of angular velocity and acceleration.

To verify the accuracy of the gyroscope sensor the 10 tablets available have been placed in a tight box not allowing any type of independent movement and were then rotated altogether by 360° using a rotating disk. As Figure 3 shows, a rotation on the tablet plane corresponds to a rotation in the z-axis relative to the coordinates of the gyroscope sensor. As the tablets are rotated, the angular velocity in the z-direction increases, before setting again to 0 once the rotation is stopped. The differences between the values recorded by each device are minimal (almost indistinguishable), giving an indication on the measurement precision. In addition, by integrating the signal obtained over the whole time period the measured angle can be obtained. In this case the recorded value was $359.56 \pm 2.12°$ suggesting that both precision and accuracy of the angular velocity measurement can be assessed as below 1%.

[2] In the crowd experiments described later a copy of the data sent over WiFi was locally stored inside each tablet to unsure that data would not get lost during communication problems. Internal data were ultimately combined with signals sent over WiFi to fill eventual gaps. However, we found data loss a quite insignificant issue (less than 1% of data got lost in communication).

[3] It is not clear which algorithm is used to perform this calculation, although different informal sources reveal that a Kalman filter is employed.

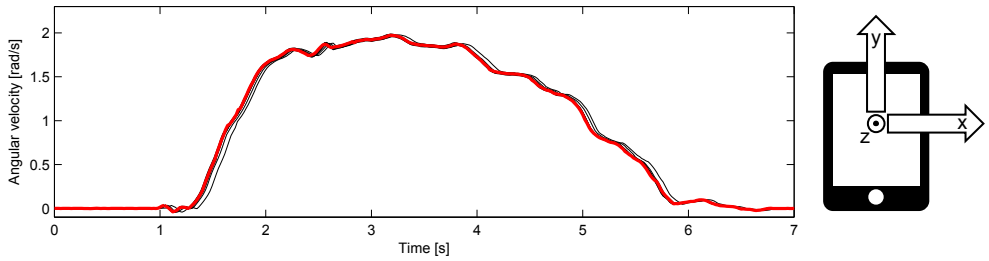

Figure 3. Measurement of angular velocity (in the z-direction) during a 360° turn using 10 Nexus 7 (2013) tablets. Each line corresponds to a single device, red line is the average among all of them.

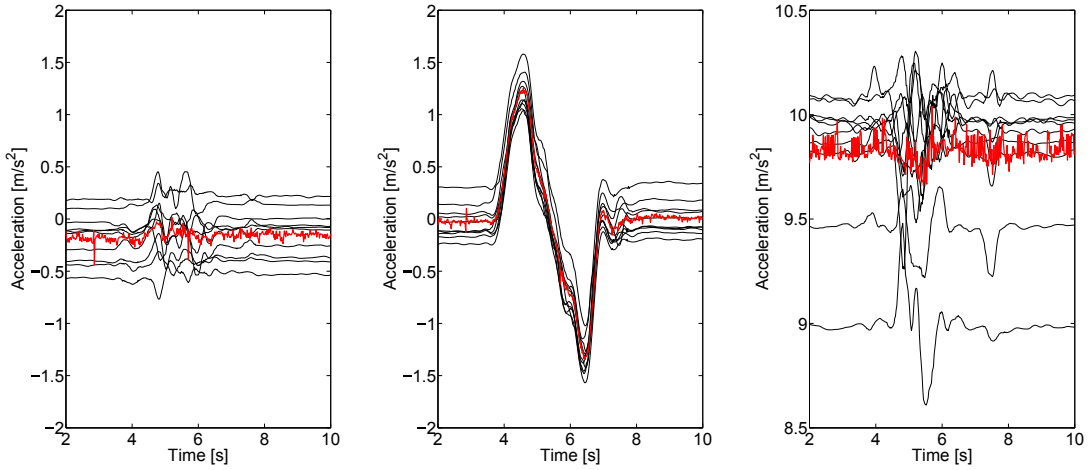

(a) x-direction. (b) y-direction. (c) z-direction.

Figure 4. Results for the acceleration/deceleration experiment using a dolly cart gained from the accelerometer of Nexus 7 (2013) tablets. Red line corresponds to the average result. Time interval has been chosen to cover the most relevant moments.

What is also important, is that, at still, the signal for the angular velocity oscillates around zero, meaning that integral value should be also close to zero (remember that integral quantities are generally used when dealing with inertial sensors and pedestrians). In addition, we found no significant variation for the angular velocity recorded in the x- and y-direction when the rotation was imposed on the z-axis.

The reasons for choosing this validation method are multiple. First of all, it is a very simple and inexpensive way for checking the accuracy of the gyroscope sensor. Secondly, the method relies on a different and independent measuring principle since angle is physically obtained. Using a specialized equipment to compare measurements from tablets' sensors would have been more expensive while measuring principles of both devices are similar, thus making them partially dependent. As a last point, the integral method allows to verify accuracy of the gyroscope and the clock together as the correct angle is obtained only if both are accurate.

To check the accuracy of the accelerometer we placed all the tablets in the same tight box used in the previous experiment and moved them on a dolly cart for 2.0 m in the y-direction (we made sure that the movement was parallel to the y-direction and perpendicular to both x- and z-directions). During the whole process, z-direction has been measuring the gravity. Figure 4 shows the results for this simple experiment in the three axes of the accelerometer.

In the y-direction it is possible to see that a positive acceleration is followed by a de-

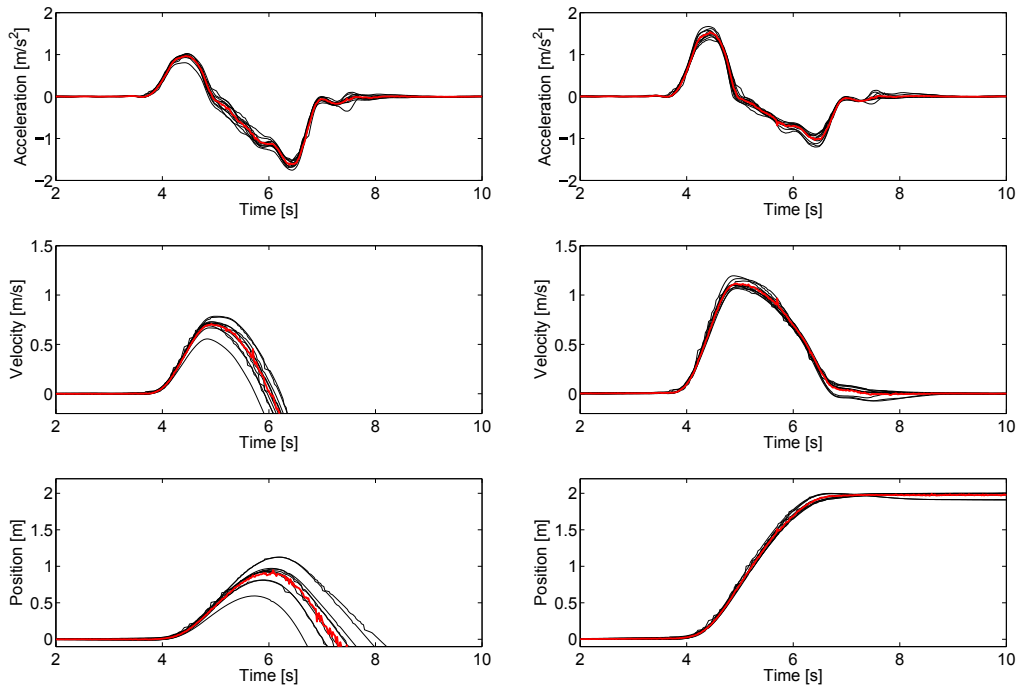

(a) Before calibration.

(b) After calibration.

Figure 5. Acceleration, velocity and position for the dolly cart experiment to test the accelerometer. Velocity and position are obtained by successive integration of the acceleration signal. All graphs refer to the y-direction.

celeration, corresponding to the translation movement performed with the dolly cart. However, what is clear from the three axis is that acceleration at still (i.e. before and after the translation) is not zero and it is not even equal among the different tablets. This does not allow an integration of the signal to obtain more important properties, since the integration would result in a continuous movement (although tablets were at still). From the z-direction it is also seen that gravity is not correctly measured, although most of the tablets are around the correct value (approximately 9.81 m/s^2). In fact, by taking the magnitude at still, the average value among the different tablets was 9.811 ± 0.340 m/s^2, quite consistent with the gravitational acceleration.

As introduced earlier, the Android OS also provides an additional "virtual" measure removing the gravitational component from the acceleration. The results for the "linear acceleration" in the same dolly cart experiment described above are given in Figure 5.

In the acceleration graph of Figure 5(a) is clearly seen that by using the linear acceleration a zero value is reported at still (before and after the experiment). We found similar results in the x- and z-direction, thus confirming that the OS filter allows to detect accelerations only when movements are actually performed. However, by integrating the y-acceleration to compute the moving velocity, we found that speed does not return to zero when the cart is at still (this also results in the changing position at the end of the experiment). We found that the reason for this fault calculation of velocity (and the distance traveled) is that positive acceleration had been underestimated (compared to deceleration). To fix the inaccuracy it is possible to determine (a posteriori) how much one would have to multiply the positive and negative acceleration to get the correct distance. By proportionally increasing the positive acceleration and reducing the negative one we were able to obtain the correct distance traveled

Table 3. Inertial sensors available in Nexus 7 (2013) devices and their characteristics. Conclusion refers to their potential use for estimating pedestrian properties.

Sensor	Gyroscope	Accelerometer	
Measure	Angular velocity	Raw measurement	Linear acceleration
Type	Sensor reading	Sensor reading	OS generated
Maximum rate	200 Hz	200 Hz	50 Hz
Precision	$< 1\%$	$< 5\%$	$< 10\%$
Accuracy	$\ll 1\%$	Largely inaccurate [a]	Largely inaccurate
Conclusion	Suitable	Unsuitable	Suitable for comparison

[a] Acceleration magnitude (gravity) measured at still was 9.811 m/s^2, resulting in an accuracy of less than 1%.

(2.0 m) as presented in Figure 5(b). However, this "corrective" gain (i.e. the multiplication factor) was not constant and it had to be changed each time the experiment was repeated. This shows that reduction of the reported "linear acceleration" may be related to its magnitude and is created by the filter applied on raw measurements.

To summarize, the results obtained from these two simple validation experiments are given in Table 3.

The gyroscope has been found being an accurate scientific instrument, with a high precision and very high accuracy. Also, its maximum sampling rate is 200 Hz, safely allowing to record also very fast movements of pedestrians. On the other side, we had to exclude the acceleration (i.e. the reading from the sensor including gravity) as a candidate to be used in pedestrian crowds. The main reason for excluding this type of measurement is that we found that acceleration does not return to zero at still, potentially allowing erroneous estimation of crowd state. Also, the direct subtraction of gravity can be difficult, since values are not constant among different devices.

However, we found that the "virtual" linear acceleration can still be useful although we had to conclude that values returned are an estimation of the acceleration and not an accurate measurement. Important for the aim of this research is that integration of linear acceleration signal at still gives zero, thus correctly indicating no movements. In addition, as Figure 5 shows, all the tablets recorded a very similar acceleration signal, so although not accurate in absolute (and physical) terms, it still allows a precise estimation of the magnitude of motion in comparative terms.

4. Testing under continuous motion conditions

To test the equipment described above with the aim to measure crowd properties, several experiments were set up. In the first experiment, very detailed information was known regarding type of device used, location where it has been stored by pedestrians and position of each participant during each moment of the experiment. Gradually, we tried to test more realistic conditions, by using different devices belonging to the participants and asking them to keep them in the usual location. Also, in the last experiment individual recognition has not been possible, with the whole crowd considered as a uniform entity. Some of the experiments considered in this section have been also analyzed under a different perspective in (Feliciani and Nishinari 2018; Feliciani et al. 2019), so readers interested in aspects related to crowd modeling are referred to those works.

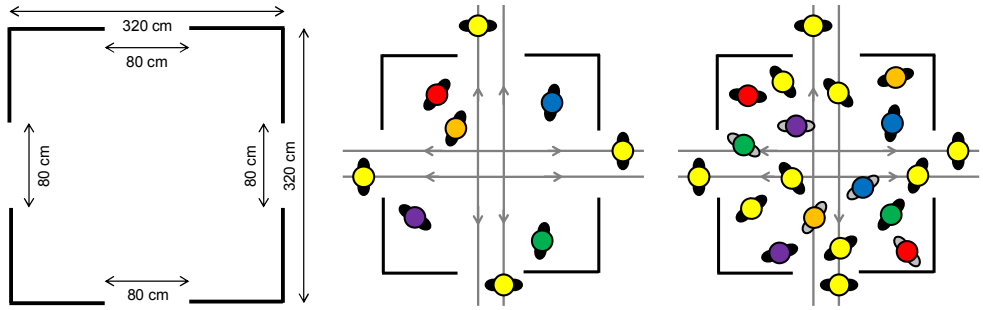

(a) Scenario dimensions. (b) Low density. (c) Medium density.

Figure 6. Configuration for the first experimental campaign testing crowd measurement under continuous and constant conditions. Participants being outside the room are the crossing pedestrians continuously going from one side to the other. People inside the room were simply asked to walk all the time without stopping.

4.1. *First campaign*

4.1.1. Experimental design

To gain experimental data over a long time and under different densities we designed an experiment where pedestrians keep moving all the time, but changes are not observed in the way people move or how organized their movements are. A room having the dimensions given in Figure 6(a) has been created delimiting each side using band partitions. Participants were asked to move inside the room for the whole length of the experiment, only stopping when instructed to do so.

Since the goal of this first test was to gain data under stable conditions in terms of both speed and density, we made sure that organizational changes do not occur during the experiment. Karamouzas et al. (Karamouzas, Skinner, and Guy 2014) predicted using a simulation model that when people move randomly in a closed room, a rotational motion around the center may arise on the long run. Although experiments considered here were much shorter than the simulations by Karamouzas et al., we added a condition to make sure that movements by pedestrians were less predictable as possible.

In particular, we asked to some of the participants to cross the room while the rest was randomly moving within it. Figure 6(b) and Figure 6(c) provide an illustrative description of the methodology used to increase congestion. Crossing pedestrians were asked to cross the room from one side to the other, briefly step out and later cross the room again in the opposite direction.

This experiment was repeated several times by gradually increasing the density. However, when changing the number of people two different strategies were employed. Under configuration A both the number of participants moving inside the room and the ones crossing it were increased at each density step. As Table 4 shows, in configuration A, the number of transiting participants has been increased by 4 (one for each side) and the number of participants moving inside the room by 5 at each step. In the first run (configuration A1) transiting participants were not present to test low density conditions. In configuration A (except A1) the ratio between pedestrians moving inside the room and transiting ones was therefore constant.

To increase the number of density steps, an additional configuration has been tested in which the number of transiting participants had been kept constant at 4 and only the size of the crowd moving inside was changed. In configuration B (whose details are also given in Table 4), 5 people were added at each repetition, increasing pedestrian

Table 4. Details on experimental configurations A and B. In the "free" configuration participants were asked to walk in an undetermined space inside or outside the experimental area (density is an estimation for this case). Also, we should remind that since no walls were employed in the experiment, high densities are likely to be overestimated. Each case was repeated only once.

Configuration (code)	Participants and role		Total	Density [m^{-2}]
	Moving inside	Side to side crossing		
A1	5	0	5	≈ 0.49
A2	5	4	9	≈ 0.88
A3	10	8	18	≈ 1.76
A4	15	12	27	≈ 2.64
A5	20	16	36	≈ 3.52
B1	5	0	5	≈ 0.49
B2	6	4	10	≈ 0.98
B3	11	4	15	≈ 1.46
B4	16	4	20	≈ 1.95
B5	21	4	25	≈ 2.44
B6	26	4	30	≈ 2.93
B7	31	4	35	≈ 3.42
B8	36	4	40	≈ 3.91
Free	–	–	5	≈ 0.1

(a) Low density (B1). (b) Medium density (B4). (c) High density (B8).

Figure 7. Examples for video frames taken at different densities; codes refer to the notation of Table 4.

density at each step by about 0.5 m^{-2}. In both configurations a maximum density close to 4 m^{-2} was reached.

Finally, to study pedestrian motion at very low densities, we asked to 5 participants to move freely around or inside the experimental area. At that time the remaining participants already left the site so the remaining 5 people could walk without (or with very limited) obstruction. Under these circumstances we were not able to accurately measure density (which has been measured using Voronoi cells (Steffen and Seyfried 2010) for configurations A and B), but we estimated that the 5 people walked in a 50 m^2 surface, thus corresponding to a density of about 0.1 m^{-2}.

To monitor movements of pedestrians and later gain their trajectories during the experiment a camera was fixed right above the center of the room at an height of around 5.5 m. Recordings were taken at 30 fps with a resolution of 1920 $\times$ 1080 pixels. Figure 7 provides some frames taken for the experiment under different densities. From Figure 7 it is seen that a rather large distortion is caused by the use of wide angle lens. Trajectories were obtained using PeTrack software (Boltes et al. 2010; Boltes and Seyfried 2013) which fixes the distortion and allows to compute trajectories using the color of participants' hats.

Among all participants 10 individuals were randomly chosen to carry tablets. A

Table 5. Combination of colors to link participant ID with tablet ID used during the experiment. Participant height is given in bracket. Participants carrying tablets were changed during the break between configurations A and B.

Tablet ID	Color		Participant ID (height)	
	T-shirt	Cap	Configuration A	Configuration B [a]
1		Blue	1 (174 cm)	11 (168 cm)
2		Green	2 (173 cm)	12 (172 cm)
3	Black	Purple	3 (172 cm)	13 (169 cm)
4		Orange	4 (164 cm)	14 (161 cm)
5		Red	5 (174 cm)	15 (182 cm)
6		Blue	6 (180 cm)	16 (162 cm)
7		Green	7 (175 cm)	17 (175 cm)
8	Gray	Purple	8 (167 cm)	18 (173 cm)
9		Orange	9 (177 cm)	19 (167 cm)
10		Red	10 (175 cm)	20 (168 cm)

[a]During the last free configuration the same setup for B was used concerning tablet numbers and T-shirts/caps color.

wearable bib with a zip pocket was used to fix the tablets on the chest of the participants (see also Figure 10). After wearing the bib, it was tightened (not too tight to still allow natural movements), with the tablets therefore measuring the motion of that portion of body between the chest and the belly. Participants were obviously aware that tablets were used in the experiment, but they were not informed in regard to which data will be extracted from the devices and which kind of sensors are contained within them. Tablet-equipped participants have been always moving inside the experimental area (they never took the role of crossing pedestrians).

Participants using tablets wore caps with colors different from yellow to allow a quick recognition. From Figure 7 it can be seen that a range of colors has been used with T-shirts also changing from gray to black. The combination of cap and T-shirt color allows a further identification of participants using tablets, eventually linking individuals (participant ID) with tablets based on the information contained in Table 5.

By taking Table 5 as reference it is possible to know that, for example, the purple cap wearing a gray T-shirt in Figure 7(b) (experiment B4) uses tablet ID 8 and was the participant having ID 18. In addition, participants were asked to provide their height at the beginning of the experiment, so we can also know that the participant taken as example had an height of 173 cm.

In total, 42 male university students took part to the experiment and received a fixed amount of money as remuneration. Average age among participants was of 20.55 $\pm$ 2.10 years and average height (including those not wearing tablets) was of 170.4 $\pm$ 5.5 cm. Although the experiment was performed outdoor the location ensured a protection from direct sunlight (it was performed in June with a temperature of about 25°C).

Instructions given to participants were simple and minimal, only asking them to walk from the "go" signal (given when the experiment was started) until the "stop" signal (given when enough data were collected). Participants did not know the aim of the experiment nor the kind of data collected. Each experiment from Table 4 was only repeated once and lasted roughly two minutes. Staff was present on-site to avoid, in particular, that crossing pedestrians would take too much time before re-entering the room.

Finally, some details are provided on the method used to synchronize tablets with

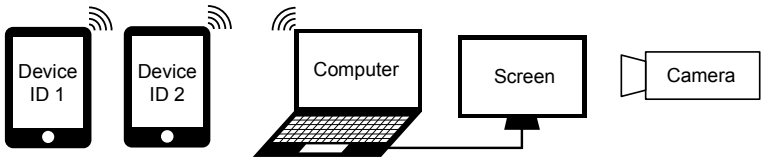

Figure 8. Schematic representation of the whole synchronization process. PC is used as reference time and inertial data from tablets are sent using a wireless network. An external screen showing time and changing color regularly is used to synchronize PC with the camera.

Table 6. Time synchronization between camera and PC reference time (difference is 1.48 s in this example). "Color change" refers to the background color of the external screen in Figure 8.

Device	Event	Internal time	Video recording (at 30 fps)	
			Time	Frame number
PC	Record start	10:27:35.67		–
Camera		10:27:37.15	0.00	1
PC	Color change	10:27:40.00		–
Camera		10:27:41.48	4.33 s	131

camera (which ultimately provides video used to gain trajectories). We already discussed the method used to synchronize several tablets (data are simultaneously send over a wireless network), but perfectly combining pedestrian trajectories and body movements is also important and requires an accurate synchronization between camera and tablets.

Since readings from inertial sensors are streamed to a central PC for storage it is important to read the time of that PC from the camera. On that purpose, an external screen was connected to the central PC continuously showing its time to the camera (this screen can be seen in the lower-left side of Figure 7). Because of its size and the resolution of the camera it was not always possible to clearly read the time and therefore an additional solution was employed.

Camera's time and PC time were manually synchronized at the beginning of the experiment with an accuracy in the order of few seconds. Background color of the external screen was changed every 10 seconds (with the zero reference set at midnight), thus allowing to determine the PC time also from distances where numbers cannot be read clearly (by knowing the approximate time and the frame at which color was changed exact time can be determined). An example for synchronization between PC and camera is given in Table 6. This system was already tested in the past (Feliciani and Nishinari 2016; Yanagisawa et al. 2016; Yamamoto et al. 2017) showing that, as a whole, the synchronization error between the different tablets and the trajectories is of $\pm$ 1 frame, equivalent to about 0.03 s. A schematic representation of the technical system used to record, store and synchronize inertial movements measured from tablets is given in Figure 8.

4.1.2. Results and discussion

In all the experiments, a stable speed was quickly reached few seconds after the "go" signal. The example provided in Figure 9(a) shows the average velocity throughout the full length of the experiment for three cases (the same provided in Figure 7). Velocity is computed from the analysis of trajectories gained from the videos. Since very stable levels of speed were maintained until shortly before the end of the experiment [4], we

[4]In B1 the number of participants is only 5, making fluctuations larger.

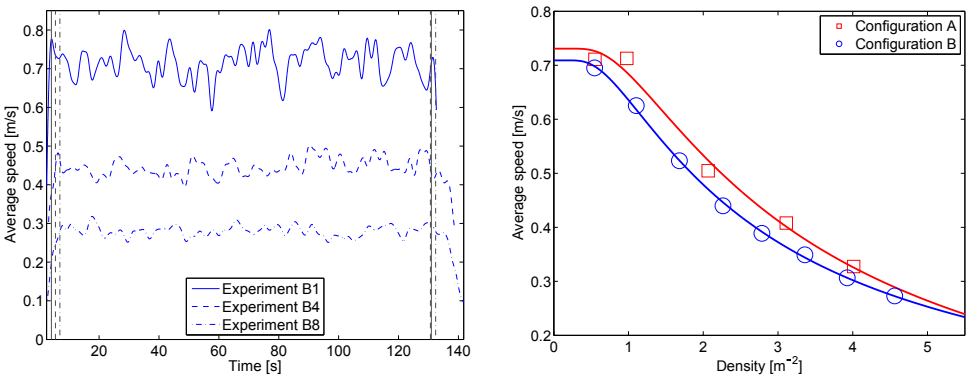

(a) Speed profile in 3 cases.

(b) Fundamental diagram (speed vs. density).

Figure 9. Temporal variation of the average speed during the execution of 3 experiments and fundamental diagram showing the relationship between average speed and density. Fitting function is the equation by Weidmann (Weidmann 1993).

decided to focus our analysis on the central part, taking a time interval specific for each case as shown by the vertical lines of Figure 9.

By taking average speed and density for each case it is possible to plot the fundamental diagram as given in Figure 9(b). Clearly, velocity drops when density increases with the dependance described well by the Weidmann equation (Weidmann 1993), given by:

$$v(\rho) = v_{max}\left[1 - \exp\left(-k\left(\frac{1}{\rho} - \frac{1}{\rho_{max}}\right)\right)\right] \tag{1}$$

where v_{max} is the maximum velocity (or free walking speed), ρ_{max} the maximum density (when motion ceases) and k an experimentally determined parameter. Although (1) fits well with both configuration A and B, the parameters used in the equation are much different from the one reported by Weidmann, meaning that the relationship between speed and density may not be universal.

Next, we can consider the results gained from the inertial sensors, which is the aim of this work. Figure 10 provides an example for angular velocity and linear acceleration measured on a pedestrian walking in an uncongested undetermined path.

In Figure 10 it is seen that the angular velocity shows a regular pattern with oscillations in x-direction, which are relative to the movements of the shoulders. Some oscillations in y-direction are also observed, which are related with the forward motion in steps. Rotations in the z-direction are minimal. It is also seen that a long term pattern is observed in x, with the values of the angular velocity taking slightly negative values before 7.5 s and changing into a mostly positive pattern later. From simple geometrical considerations we know that by turning with a constant radius in the clockwise direction a negative background angular velocity will be generated. In addition, the movement of the shoulders is superimposed creating the oscillatory pattern. A counterclockwise turn generates a background positive angular velocity in the x-direction, with the signal being larger for high turning speeds. To conclude, we can state from the analysis of Figure 10 that the considered pedestrian was taking a S-curved path and changed the direction at around 7.5 s.

As it can be seen from Figure 10, values relative to the linear acceleration seem to

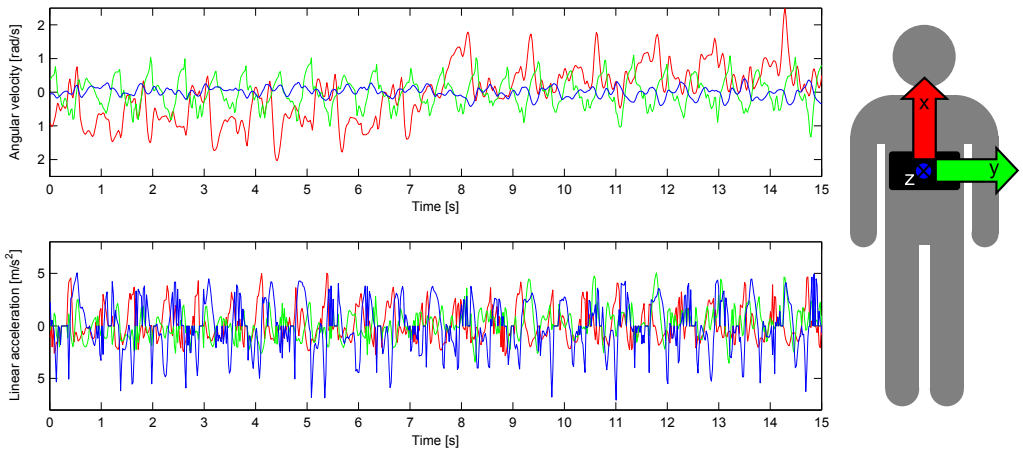

Figure 10. Example for angular velocity and linear acceleration taken during the "free" experiment. From the angular velocity it can be guessed that the participant was taking a slightly turning S-shaped path.

be less dependent on the walking direction [5]. Remarkable is the acceleration in the x-direction which takes mostly positive values. This is understandable by considering that a larger acceleration is achieved when movements are directed toward the ground, with upward movements requiring physical efforts and being therefore slower. On the other side motion in y- and z-direction which is less dependent on gravity is more uniform.

We can finally consider the measurements from inertial sensors taken during the crowded experiments, with a representative example provided in Figure 11.

From Figure 11 it can be observed that the regular patterns observed earlier disappear when interactions with other pedestrians become strong. In particular, rotational movements measured by the gyroscope become large with the x-direction (main axes of the body) taking large values. It is now possible to recognize strong body rotations, which are necessary to avoid other pedestrians or to change direction while approaching the wall. For both the gyroscope and the accelerometer, oscillations tend to be large in experiment B1, where densities were low.

To compare the different configurations more efficiently, it is convenient defining a unique measure estimating the "amount of body motion". This can be done by taking the average absolute value for each signal or, in mathematical terms:

$$\overline{x} = \frac{\int_{t_0}^{t_1} |x|}{t_1 - t_0} \tag{2}$$

where x is the analyzed signal (angular velocity or linear acceleration in one direction) and t_0 and t_1 are the integration limits. From here on we will focus on this measure and see how it changes in the different configurations.

As mentioned earlier, Mori et al. (Mori et al. 2013) used the maximum of the vertical acceleration to determine if people were running, walking or stopped. In our analysis we will use the average vertical acceleration (obtained based on (2) and using start and end times as indicated in the example of Figure 9(a) as integration limits) and compare it with the walking velocity obtained by tracking each pedestrian individually.

[5]Nonetheless, we should remind here that gravity is subtracted by calculation and therefore accuracy may depend on the orientation of the tablet (and ultimately the sensor).

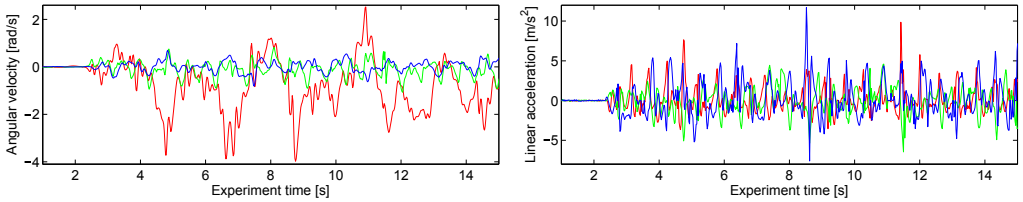

(a) Configuration B1.

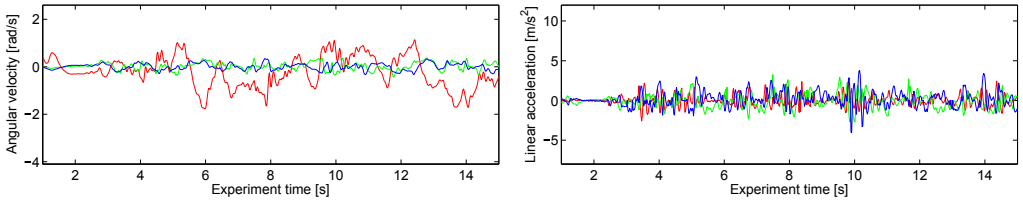

(b) Configuration B4.

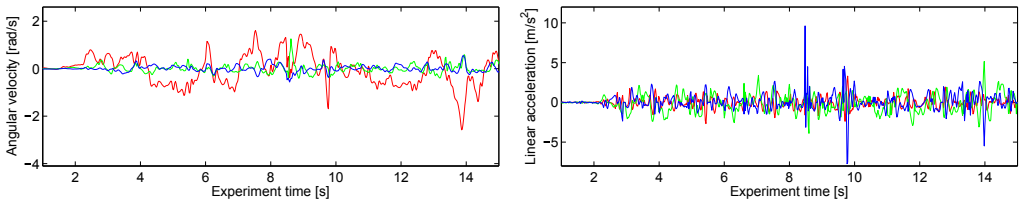

(c) Configuration B8.

Figure 11. Measurements from inertial sensors by the same person during three different experiments (examples provided here corresponds to the cases given in Figure 9(a) and Figure 7). Colors refer to the orientation provided in Figure 10.

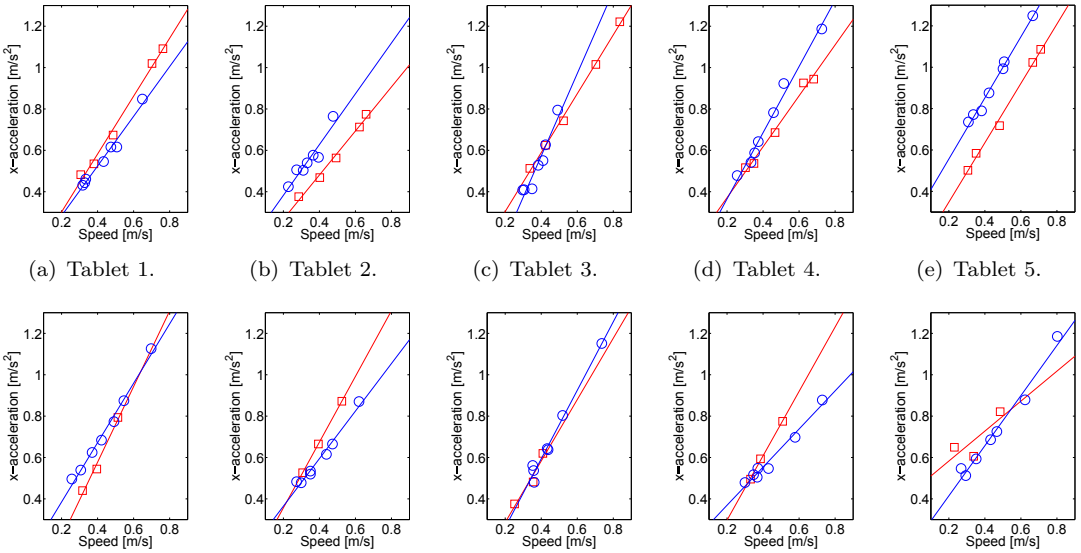

(a) Tablet 1. (b) Tablet 2. (c) Tablet 3. (d) Tablet 4. (e) Tablet 5.

(f) Tablet 6. (g) Tablet 7. (h) Tablet 8. (i) Tablet 9. (j) Tablet 10.

Figure 12. Relationship between individual walking speed and body acceleration in the x-direction (vertical direction) for configuration A (red squares) and B (blue circles).

Results are presented in Figure 12 for all individuals carrying tablets.

Since participants using tablets were changed from configuration A to B, both cases are not directly comparable for this type of analysis. It is seen that walking speed fits comparatively well with the acceleration of the body in the vertical direction (especially for configuration B which has more data), showing that under the experimental conditions tested here a more accurate prediction of velocity is possible compared to the three-states categorization by Mori et al. (Mori et al. 2013). Furthermore, we also partially confirmed that linear acceleration can be effectively used despite its limitation in not providing "real" values for acceleration. By checking different quantities such as the angular velocity in x-direction (yawing), we found that similar results are found and a linear trend with speed is seen in all the cases. In addition, we also found that by taking magnitude values (i.e. combining all directions) only minor changes were observed in the results. This observation is important, since in reality it cannot be known where people keep their electronic devices while walking and therefore only magnitude can be used in those cases.

From Figure 12 it is also seen that, although a linear trend is found for all participants, slopes are not equal. In a first guess, trying to understand those differences, we checked the relationship with body height, but we found no significant correlation. However, we found that, when the measurements from the different tablets are combined and compared with crowd quantities such as group average speed and density, then individual differences are not very significant. Figure 13 presents the relationship between average crowd walking speed and density toward linear acceleration and angular velocity (magnitudes are used here in all the cases).

In Figure 13 we decided to consider both configurations together for two main reasons: (i) because the differences are not large (especially in the case of density) and (ii) because the final aim is to estimate general crowd properties based on inertial measurements. To evaluate speed, a linear function was found fitting well with experimental data, while for density a power function had to be used.

The fitting values provided in Table 7 allow to do some remarks on the behavior

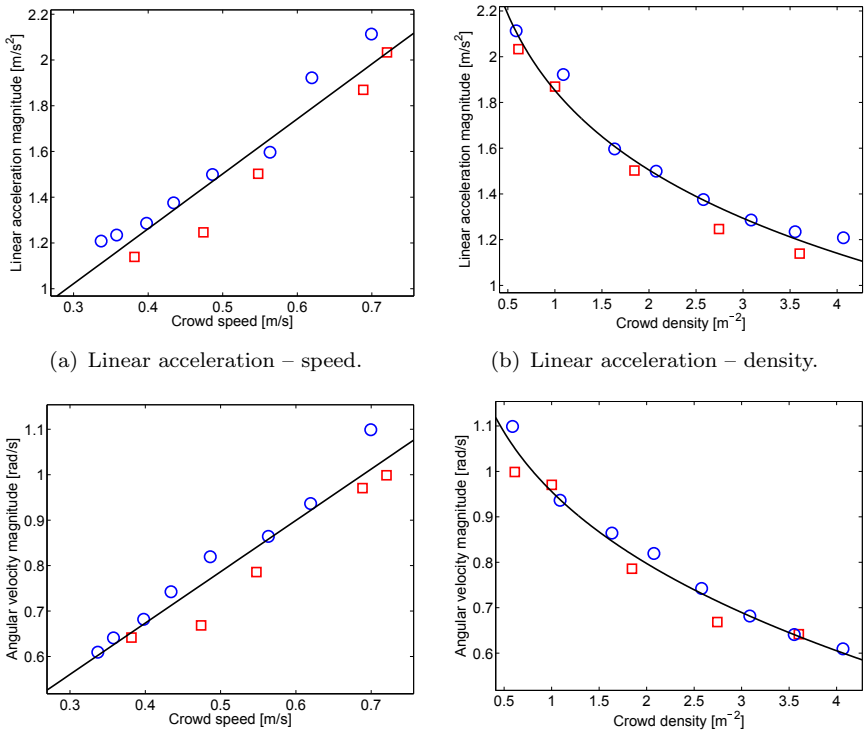

(a) Linear acceleration – speed.

(b) Linear acceleration – density.

(c) Angular velocity – speed.

(d) Angular velocity – density.

Figure 13. Relationship between crowd quantities measured using computer vision and inertial measurements on pedestrians. Red squares belong to configuration A, blue circles to configuration B. Fitting functions and parameters are given in Table 7. In all the cases magnitude was used, i.e. the three directions from the inertial unit were combined.

Table 7. Fitting parameters for the graphs provided in Figure 13. s refers to the quantity measured from the sensor (magnitude in all cases), x to the crowd measure. Units are omitted in the fitting parameters for convenience. R^2 is the coefficient of determination.

Crowd (x)	Inertial sensor (s)	Function $s = f(x)$	Fitting parameters p_0	p_1	p_2	R^2
Speed	Linear acceleration	$s = p_0 x + p_1$	2.033	0.573	–	0.928
	Angular velocity		0.953	0.351	–	0.927
Density	Linear acceleration	$s = p_0 x^{p_1} + p_2$	-2.750	0.154	4.602	0.975
	Angular velocity		-0.499	0.357	1.455	0.972

Table 8. Quantities relative to crowd and body motion during the free walking experiment. Walking speed could somehow be measured, density is guessed intuitively. Magnitude values are used for inertial measurements.

Quantity	Result	Mode
Walking speed	≈1.0 m/s	Partial measurement
Density	≈0.1 m^{-2}	Rough estimation
Linear acceleration	2.655 m/s^2	Measurement
Angular velocity	0.708 rad/s	Measurement

of crowds at particularly high densities. The function used for speed leads to the conclusion that also when crowd speed is zero, some sort of oscillatory movements are expected from the people since intercept (parameter p_1) for both linear acceleration and angular velocity is positive. The expression for density leads to the same qualitative conclusion, i.e. that at very high densities acceleration and angular velocities are still positive (complete stop is found at a density of 28.32 m^{-2} and 20.04 m^{-2} for acceleration and angular velocity respectively). While the range of speeds and densities considered here may not be sufficient to come to this sort of conclusions, these remarks are in line with observations during accidents which noted that pressure waves occur with people practically staying in the same position all times (Helbing, Johansson, and Al-Abideen 2007).

In the analysis performed so far the last free walking experiment has not been considered yet (excluding for the graphs in Figure 10). While density could not be measured accurately, we were able to partially measure walking speed in the moments when participants transited below the camera (resulting in a speed of around 1 m/s). Body motion was however accurately measured all the time (tablets continuously streamed inertial measurements even when participants were away from the camera's field of view) and results for both quantities are given in Table 8.

By comparing the results from Table 8 with the graphs presented in Figure 13 an important consideration has to be made. While the value for the linear acceleration is consistent with the fitting functions obtained, predicting a very low density (0.106 m^{-2}) and a relatively high walking speed (1.086 m/s), the measurement from the gyroscope seems not to follow the behavior described so far (0.708 rad/s corresponds to about 0.4 m/s). The reason for this prediction failure is that, during the free walking experiment, participants mostly walked straight, turning much less compared to the motion inside the room. This relates to lower values for the angular velocity. A conclusion from this observation is that while both angular velocity and linear acceleration are valid under comparable scenarios, only the linear acceleration is universal in respect to pedestrian crowds and route choice. This could also be the reason which led Mori et al. to focus on the accelerometer in judging moving states during emergencies

(although the reason is not clearly stated in their work). For the reasons discussed above, we will focus on the linear acceleration from now on and, considering practical applications, we will always use the magnitude to exclude device orientation issues.

4.2. *Second campaign*

4.2.1. Experimental design

The experiments presented so far showed that inertial sensors contained in commercial devices allow to get aggregated but yet significant information on crowd motion. However, the methodology tested so far cannot be applied to real conditions, since, in general, it is not possible to know in advance the position and the orientation of the device used. Also, hardware varies greatly from person to person, with some devices using highly accurate sensors for gaming requirements and others making use of low cost sensors for basic functions only. In addition, in the experiments described earlier, only densities above 0.5 m^{-2} have been accurately studied. While the overall focus of this work is mostly on dense crowds, it is also important to notice that most of the public spaces are not extremely crowded. As a consequence of these arguments, a second experimental campaign was conducted, including very low densities conditions (while also including heavily crowded scenarios) and having a part of the participants using their own phones in an effort to reproduce more realistic conditions.

Geometry and procedures for this second experimental campaign were very similar to the previous one. The main difference concerns the strategy used to change density: in this second campaign both the number of participants and the size of the room have been changed. In particular, two room configurations were used: a wide room (taking the whole surface available, equivalent to 96 m^2) and a narrow room whose surface had been gradually reduced from 36 m^2 (side length 6 m) to merely 9 m^2 (side length 3 m). Both experimental setups are schematically illustrated in Figure 14.

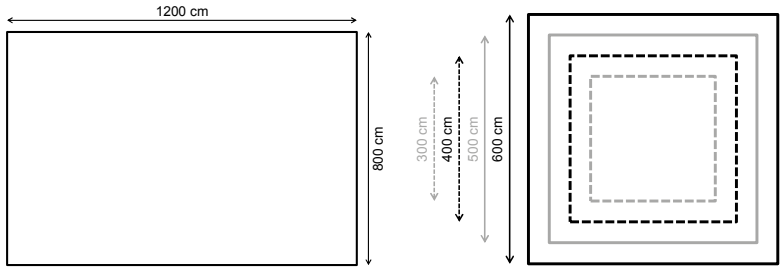

(a) Wide room. (b) Narrow room.

Figure 14. Geometry used during the second experimental campaign. In this case crossing pedestrians were not present, so gates do not exist in the middle of each side.

Qualitative and quantitative analysis of the trajectories obtained from the first experimental campaign showed that, in contrast to what Karamouzas et al. predicted, circular motion did not occur or, more probably, the time was not long enough to have this kind of self-organization. For this reason, we decided to keep the experimental setup as simple as possible and only pedestrians moving inside the room are considered here.

This second campaign was performed half a year later with different participants but recruited using the same modality (i.e. paid university male students who voluntarily applied for the experiment). Instructions given to them were also the same: keep

Table 9. Details for the second experimental campaign. In total 42 participants took part to the experiment and about half of them were equipped with devices measuring their body movements. Tablets were positioned to monitor the motion of the chest as in the previous campaign, position of smartphones are given in Table 10. Also in this case, we should remind that since no walls were employed in the experiment, high densities are likely to be overestimated.

Configuration (code)	Participants and sensor				Area [m^2]	Density [m^{-2}]
	Smartphone	Tablet	No sensor	Total	Size [m]	
C1	5	0	0	5	96 (12 × 8)	≈ 0.05
C2	10	0	0	10	96 (12 × 8)	≈ 0.10
C3	10	10	0	20	96 (12 × 8)	≈ 0.20
C4	10	10	10	30	96 (12 × 8)	≈ 0.31
C5	10	10	22	42	96 (12 × 8)	≈ 0.44
C6	10	10	22	42	36 (6 × 6)	≈ 1.17
C7	10	10	22	42	25 (5 × 5)	≈ 1.68
C8	10	10	22	42	16 (4 × 4)	≈ 2.63
C9	10	10	22	42	9 (3 × 3)	≈ 4.67

waking without stopping until the end of the experiment. Number of participants and geometrical setup used for each execution (performed once) are given in Table 9 (we will call this configuration with the letter "C" to distinguish it from the previous ones).

As shown in Table 9, 20 participants used electronic devices containing inertial sensors to measure body motion. 10 of them were equipped with Nexus 7 (2013) tablets provided to them for the scope of the experiment. Position and configuration of those tablets has been the same for the experiments presented so far, with the device being positioned around the chest monitoring the motion of the central-upper part of the body. Participants carrying tablets have been the same for the whole length of the experiment (i.e. from C1 to C9).

In addition, to test conditions similar to reality, 10 additional participants gave their consent to use their own smartphones. Due to technical limitations, only Android users were selected for this role. Devices were different from person to person and also the position used to keep them was not the same among the participants as shown in Table 10. To recreate realistic conditions, volunteers using their own smartphones were asked to keep it in the usual position, without giving them particular instructions. At the end of the experiment, we asked the position used to keep their smartphones and the answers are given in Table 10. Most of them opted for their pants pocket, although right and left side was almost split in half. Only one participant stored his phone in the pocket of his shirt. Most of the smartphones were equipped with both accelerometer and gyroscope, although ID 10 only had the accelerometer available. This also shows that for practical applications, the accelerometer may be more appropriate.

Participants using tablets and smartphones were uniformly mixed inside the crowd with normal participants not using electronic devices. Different cap colors were used to distinguish each class of participants but we did not focus on individual recognition like in the previous campaign. Blue caps were used for individuals carrying smartphones and green for the ones carrying tablets. Yellow caps were assigned to normal participants not having inertial sensors installed on them.

Extraction of trajectories has been performed using the same technique described earlier, e.g. video recordings were obtained from a camera placed in azimuthal position over the center of the room and frames were analyzed using PeTrack software. Figure 15 provides some pictures taken during different configurations. As it can be noticed, experiments for this second campaign were performed indoor. Also, distortion has been corrected in the frames of Figure 15, with the borders of the room show-

Table 10. Smartphone model, available sensors and location used to keep the phone during the experiment. Except for ID 10 all smartphones were equipped with gyroscope and accelerometer.

Phone ID	Model	Sensors		Position
		Accelerometer	Gyroscope	
1	SO-04G	Both available		Pants pocket, right
2	LGV32	Both available		Pants pocket, left
3	SO-03H	Both available		Pants pocket, left
4	SH-01H	Both available		Pants pocket, left
5	F-06E	Both available		Pants pocket, right [a]
6	SO-04H	Both available		Shirt chest pocket
7	SO-02F	Both available		Pants pocket, right
8	F-02G	Both available		Pants pocket, right
9	SO-02H	Both available		Pants pocket, left
10	HTV31	Available	Not available	Pants pocket, right [b]

[a]Problems with OS generated linear acceleration, which stopped during some of the experiments. [b]Only acceleration measured, linear acceleration was not provided and could not be used in the analysis.

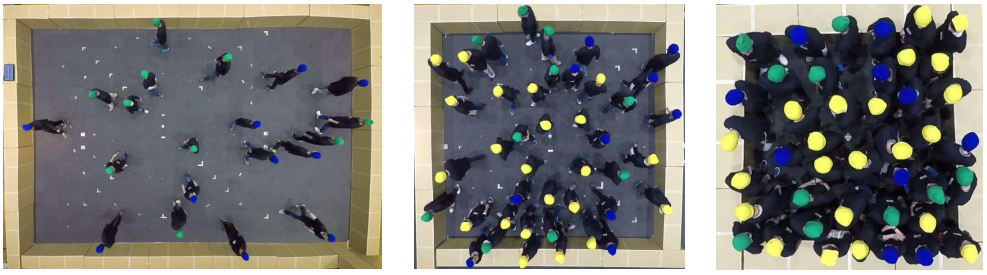

(a) Low density (C3). (b) Medium density (C6). (c) High density (C9).

Figure 15. Example of frames taken during the second campaign. Scale of each image is different as it can be guessed from the relative size of each cap.

ing fairly straight lines. Body silhouette still presents signs of distortion, but these effects are accounted by PeTrack during the extraction of trajectories, thus eventually providing the position of the feet.

Synchronization between tablets, smartphones and camera was performed using the same method described earlier (the external screen from the PC is visible on the left side of Figure 15(a)).

4.2.2. Results and discussion

Analysis of the results has been performed following the same methods presented for the previous campaign, although here we set a particular attention in understanding the influence of the electronic device used on the results. Also for this second campaign, results presented hereafter refer to the stable conditions, which were reached few seconds after the start of each execution.

Results concerning walking speed and its relationship with density (fundamental diagram) were analogous to the previous case, so we can directly consider the data gained from the inertial sensors. Figure 16 presents the relationship between (magnitude of) linear acceleration and typical crowd quantities. Graphs are divided into three groups constituting the different types of devices used: tablets only, smartphones only and all devices without distinction. As for the previous case, a linear function was found fitting well data for velocity and a power function the ones for density (fitting parameters and goodness is given in Table 11).

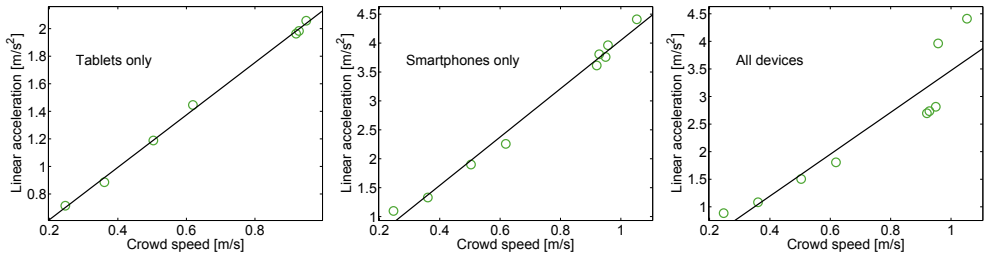

(a) Linear acceleration – speed.

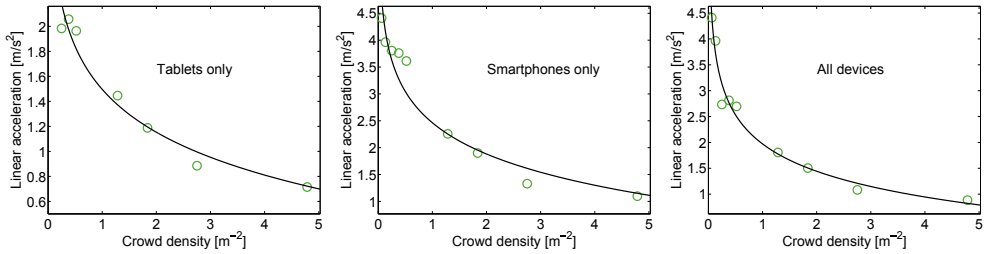

(b) Linear acceleration – density.

Figure 16. Relationship between crowd quantities measured using computer vision and inertial measurements from portable devices (magnitude is used here). Fitting functions and parameters are given in Table 11. The "tablets only" case has less density points available since C1 and C2 configurations only had smartphone participants.

Different observations can be done here concerning the results reported in Figure 16 and Table 11. First of all, it was confirmed that the gyroscope cannot provide accurate information since results are dependent on the geometry being tested and the specific position where the device is kept. From the previous campaign we know that the gyroscope fundamentally provided a measure proportional to the number of turns. Given the very specific storage location and the constant geometry, there was a relationship between number of turns and speed/density. However, this reasoning does not hold true for the second campaign since different types of "room" were used.

This is shown in Table 11, which provides in bracket the R^2-value obtained by fitting each function with the magnitude of angular velocity. In all the cases with a single exception a better fitting is used by using the linear acceleration. More importantly, it is seen that when only tablets are considered, which all had the same orientation and position, the worst R^2-values are found for the gyroscope. This is connected to the fact that geometry was changed several times during this campaign and the position of the tablets is very sensitive to these changes (number of turns now varies also because of changes in geometry). Results get better when smartphones are considered since orientation and position are more randomly distributed among the crowd. To conclude, linear acceleration was confirmed being more accurate and therefore only values relative to the linear acceleration are given for the fitting parameters in Table 11 and the graphs in Figure 16.

Concerning the type of device used and the place where it is stored, it seems that the influence is minimal as the graphs of Figure 16 show. When only tablets are considered (as for the previous campaign), then a very good fit is found for both velocity and density. But also when participants using their own smartphones are analyzed as a group, then a good fitting is found; this although models and storage locations were different. Some differences are found in the values for acceleration found among both groups, which is a result related to the position used to store the devices,

Table 11. Fitting parameters for the graphs provided in Figure 16. s refers to the (magnitude) of linear acceleration, x to the crowd measure. Units are omitted in the fitting parameters for convenience. R^2 is the coefficient of determination. Values in bracket are relative to the fitting performed using the angular velocity (whose graphs are not provided here).

Measure (x)	Used devices	Fitting function $s = f(x)$	Fitting parameters p_0	p_1	p_2	R^2
Speed	Tablet	$s = p_0 x + p_1$	1.901	0.233	–	0.998 (0.530)
	Smartphones		4.181	-0.133	–	0.989 (0.988)
	All devices		3.795	-0.323	–	0.854 (0.670)
Density	Tablet	$s = p_0 x^{p_1} + p_2$	303.7	-0.0016	-302.2	0.954 (0.459)
	Smartphones		771.0	-0.0011	-768.5	0.929 (0.935)
	All devices		8.857	-0.0888	-6.885	0.976 (0.936)

but differences should be minimal for large crowds or realistic conditions such the ones represented by the smartphones users. The different ratio of smartphones and tablet users leads to some discrepancies when the whole population of participants using electronic devices is considered, but deviations are only seen in velocity, with the fitting of density being much better.

These results show that it is actually possible to measure crowd properties based on information gained from inertial sensors also in fairly heterogeneous situations. While differences in habits among individuals considered here are relatively small (almost all participants opted for the pocket), their number was also comparatively small. In large crowd composed of several hundreds or thousands of people or very long sampling periods results with similar accuracy can be expected.

4.3. *Remarks on density estimation*

In the previous experiments both speed and density of the crowd have been estimated based on the information gained from inertial sensors. As already discussed, while the relation between walking speed and body acceleration is a consequence of human locomotion, density is only indirectly related to it through the relationship between speed and density portrayed by the fundamental diagram for pedestrian motion. In the experiments presented so far a very particular and unique type of motion was considered and therefore density and speed are closely and precisely related. But in general the relation between walking speed and crowd density is not universal and it depends on several aspects such as gender, age (Cao et al. 2016) and culture (Chattaraj, Seyfried, and Chakroborty 2009) only to list few. It is therefore questionable whether the method presented above would be applicable to real scenarios.

On this scope we collected fundamental diagrams from multiple sources and fitted each dataset using equation (1). The result is given in Figure 17(a) where the different fundamental diagrams are plotted. Although differences are seen between different authors, it can be noticed that in all the cases the Weidmann equation describes quite well the change in speed and numerical differences are limited. We can therefore consider the several datasets as variations relative to the statistical nature of human crowds. Using the fittings of Figure 17(a) it is therefore possible to plot a general fundamental diagram providing average and deviation of crowd speed at different densities, resulting in the graph of Figure 17(b).

The fundamental diagram of Figure 17(b) shows that when the crowd is not dense it is possible to associate a given speed with a limited range of densities. As the density increases, finding a relation with a specific speed becomes less accurate. It

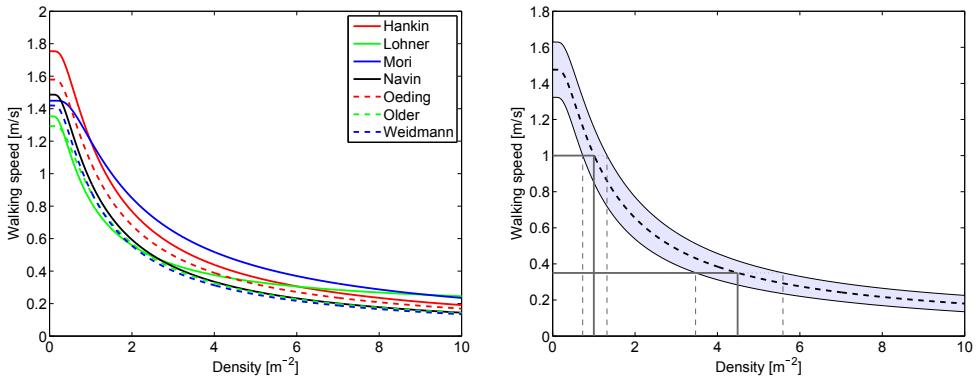

(a) Fundamental diagrams from literature.

(b) Density level estimation.

Figure 17. Fundamental diagrams from literature (Hankin and Wright 1958; Lohner et al. 2018; Mōri and Tsukaguchi 1987; Navin and Wheeler 1969; Oeding 1963; Older 1968; Weidmann 1993) and collective representation aimed at estimating the density level. R-square values for each fitting are: Hankin 0.959, Lohner 0.980, Mori 0.972, Navin 0.723, Oeding 0.714, Older 0.827 and Weidmann 0.938.

is however possible to define three density ranges with characteristic speeds. A low density region ($\rho \leq 1.00$ m^{-2}) with a speed above 1.00 m/s; a medium density region (1.00 m$^{-2} < \rho < 4.49$ m^{-2}) characterized by a speed between 0.35 and 1.00 m/s and a high density region ($\rho \geq 4.49$ m^{-2}) with a speed below 0.35 m/s. As graphically shown in Figure 17(b) the transition between low and medium density regions can be estimated with an accuracy of 0.27 m^{-2} by setting the speed threshold at 1.00 m/s. For the transition between medium and high density the accuracy is lower due to the shape of the fundamental diagram resulting in a deviation of 1.02 m^{-2} for a threshold speed of 0.35 m/s.

From the above considerations it can be concluded that while an accurate measurement of density is only possible under specific conditions such the ones considered in this work, an estimation accounting for different levels would be feasible also in more heterogeneous scenarios. In this regard, it should be also reminded that errors in the order of 10–20% are usually tolerated in the frame of data collection for city planning (Poapst 2015) and therefore density estimation using the fundamental diagram may be sufficient on this scope.

5. Application on transient scenarios

In the previous experiments we have considered only cases in which conditions did not change over space and time. Velocity and density have been fairly constant for each experimental execution and therefore we have been able to summarize each case using a single value for both. In a move toward increasingly realistic scenarios we now want to consider a different situation where both velocity and density vary.

5.1. *Experimental setup*

A room with a single exit has been setup after the experiments of the second campaign described above. The room had a width of 4 m and a length of 7 m in the middle of which a door 80 cm in width was positioned. Technical equipment and participants did not change from the previous experiment. Images of the bottleneck experiment

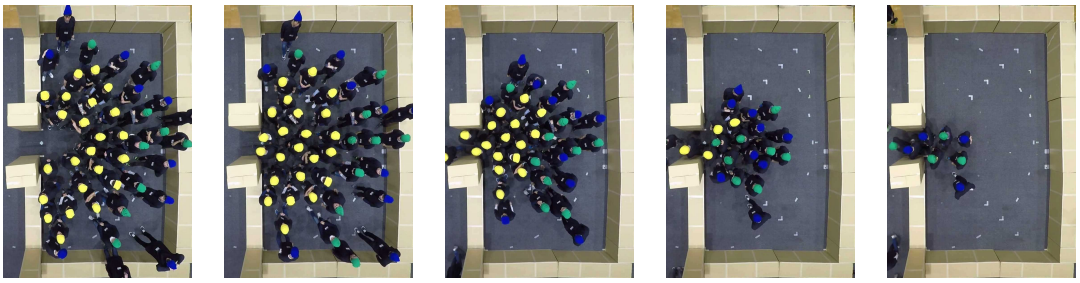

(a) Start position. (b) $t = 0$ s. (c) $t = 5$ s. (d) $t = 15$ s. (e) $t = 25$ s.

Figure 18. Example of video frames from the bottleneck experiment with 43 participants. "Start position" refers to the positions taken by participants before the beginning of the experiment. Reference time $t = 0$ is relative to the first participant crossing the exit position. Participants with green and blue caps did carry electronic devices with inertial sensors.

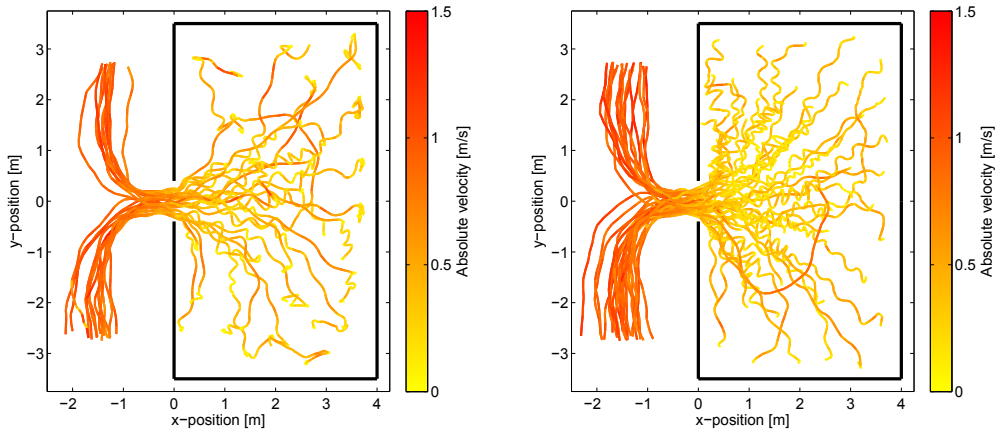

(a) 25 participants, run 3. (b) 43 participants, run 1.

Figure 19. Trajectories of the bottleneck experiment for different densities. The color used in the trajectories are relative to the walking speed, which clearly increases after leaving the room.

are provided in Figure 18.

Participants were simply asked to get inside the room and place themselves around the exit door. We tried to always have the participants not equipped with sensors waiting closer to the exit (as seen for example in Figure 18), but this instruction was not always followed correctly (resulting in a more random dispersion). After giving a "go" signal, pedestrians started leaving the room and walked away from the exit to avoid the formation of a crowd obstructing the evacuation maneuver. We asked them not to run (for safety reasons) but at the same time to leave the room as quickly as possible. The trajectories from Figure 19 and the frames from Figure 18 should help understanding the experimental procedure.

Two different configurations were tested keeping the same room but changing the number of pedestrians. A first configuration (which was repeated 3 times) had 25 participants followed by a second one (repeated 5 times) with 43 participants [6].

[6] One participant was late and did not take part to the experiments described earlier, which had 42 participants.

Table 12. Details on the bottleneck experiment. Evacuation time is computed from the first pedestrian leaving the room to the last one passing the exit door; deviation is relative to the repetitions.

Configuration	Participants				Runs	Evacuation time
	Tablet	Smartphone	No sensor	Total		
Low density	10	10	5	25	3	18.53 ± 0.47 s
Medium density	10	10	23	43	5	29.95 ± 0.82 s

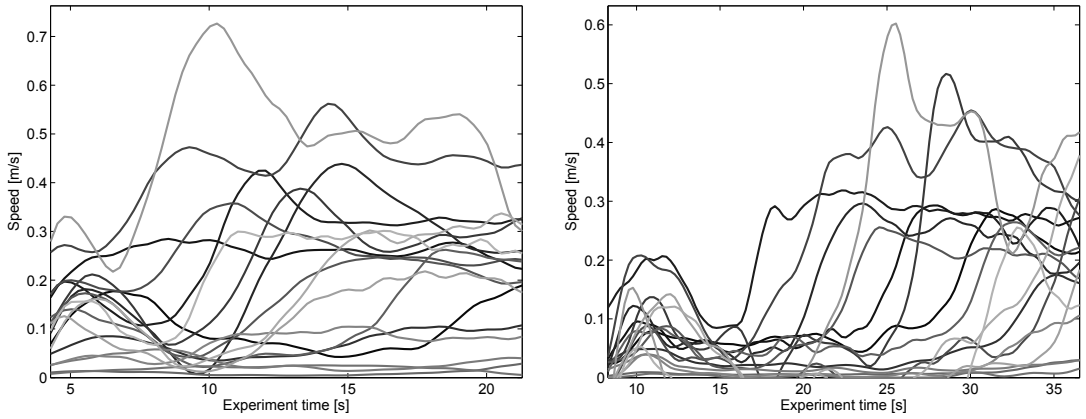

(a) 25 participants, run 2.

(b) 43 participants, run 3.

Figure 20. Speed during evacuation estimated using information from the inertial sensors. Each line correspond to a different participant. Reference time $t_0 = 0$ is set when the first participant left the room.

5.2. *Results and discussion*

Evacuation time, i.e the time passing from the first person leaving the room until the last one, is given in Table 12 for both configurations. It is interesting to notice that, although the evacuation time is obviously higher when the number of pedestrians is larger, it took proportionally less time in the second case (with the time per person being 6.4% lower than the low density experiment). This may suggest a somehow more efficient evacuation when more people were present.

We now want to consider the data gained from the inertial sensors during the evacuations tested here. Results for velocities estimated during two executions belonging to each configuration are given in Figure 20.

To compute walking velocity from inertial data the following steps has been performed. For each device a calibration has been performed using the experiments relative to the second campaign. Average values for the linear acceleration (magnitude) were computed for each experiment from C1 to C9 (see Table 9) and they were fitted against crowd velocity using a linear function (as discussed earlier). Since individual combination of trajectory and inertial data was not available here (only 3 colors for caps are used), we assumed that each pedestrian walked at the same velocity (compared to the others) during a single execution. Although we know that this assumption is not totally correct (velocities are slightly different among individuals also for the same configuration), we wanted to test a hypothetical worst-case scenario in which only aggregated data are available for calibration. After obtaining individual parameters for the (participant) linear acceleration – (crowd) walking speed relationship, we used those parameters to determine the velocity of the same individuals equipped with sensors during the bottleneck experiment.

From the results in Figure 20 it is seen that, generally, the behavior expected in case

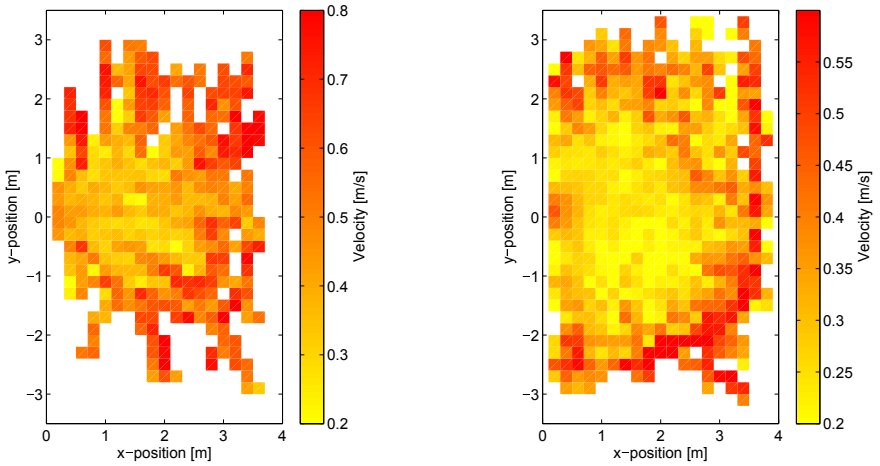

(a) 25 participants (all runs). (b) 43 participants (all runs).

Figure 21. Average velocity in different areas of the experimental area. Exit location is at coordinate (0,0) in the middle of the y-axis. In general, pedestrians move quickly toward the exit and velocities reach a minimum in a concentric region about 1 m from the exit.

of evacuation is reproduced. Results from Figure 20 are qualitatively similar to the velocity map reported in Figure 21. Pedestrians far from the exit quickly move toward the center with the highest velocities recorded at the boundaries. The lowest velocity is seen in a wide region concentric to the exit. In Figure 20(b) a minimum velocity is found at around 15–20 s, which is possibly in line with the time during which most of the participants equipped with sensors passed through the low speed region (the case represented in Figure 20(b) had a similar initial configuration to Figure 18). However, when numerical values are compared, it is clearly seen that velocity measured using sensors is far below the correct values obtained from the camera. Also, negative velocities were often obtained (theoretically impossible since estimated velocity is the absolute value) and the maximum velocity is too low (real speed was around 1.5 m/s when participants left the room, see Figure 19). In this sense, results show that while it is possible to qualitatively detect also small changes occurring over a very short time span (few seconds), quantitative results are largely inaccurate and a proper (individual) calibration would be required to correctly measure speed. Alternatively, a larger number of people equipped with sensors may help increasing the accuracy of detection, but estimating the minimum number may not be an easy task.

6. Conclusions

In this study, we considered the use of inertial sensors from commercial devices to measure properties of pedestrian crowds (in particular walking speed and density). An initial investigation on accuracy and precision of the motion sensor contained in a specific commercial device (Nexus 7) showed that while angular velocity is measured with very high precision and accuracy, accelerometer do not provide reliable data. In particular, acceleration measured at still does not correspond to gravity and also the linear acceleration provided from the OS does not represent an accurate physical measurement.

On the other side, when applied on a pedestrian crowd, we showed that the lin-

ear acceleration allows to accurately estimate walking speed for individuals and also predict with good accuracy overall crowd speed and density. While the accuracy to predict density is clearly an effect of the fundamental diagram in which both are related, the ability to estimate velocity is dependent on the performances of the inertial sensors. In addition, we showed that only the accelerometer is relevant for estimating crowd properties, since values gained from the gyroscope also depend on the geometry where people move and ultimately the route chosen.

Our research also showed that location where the device is stored plays a marginal role and in realistic scenarios where people used their own device in normal conditions we were still able to find a relationship between walking speed and amount of body motion. To conclude, we showed that a fairly simple analysis allows to get a quite accurate estimation of crowd walking speed (and density) assuming that a sufficient number of individuals are being monitored and that sampling time is sufficiently long. In that regard, applications on short transient scenarios also showed promising results, but more investigations and sophisticated algorithms are required to measure subtle changes in crowd conditions.

The system proposed here shall be seen as a technology filling the gaps found among other approaches used to estimate crowd properties. While accuracy offered by distance sensors and computer vision algorithm is clearly out of range, the flexibility of the proposed method allows to use it in a larger number of situations and in locations where sensors where not placed in the first instance. The use of inertial sensors is therefore to be seen as a rough but still reliable estimate which allows a first-hand analysis of what is happening over a large area and eventually order a more in-depth analysis if required. In particular, the method proposed here may be considered a complementary system in addition to typically used people counters to gain information on walking conditions over large areas and implement strategies for city planning and infrastructure improvements.

In the future, real crowds in public spaces could be tested to verify the efficacy of the system proposed here in practice. While this step may not be particularly challenging from a technical point of view, there may be several hurdles related to having a large number of people using the system in a limited space. While volunteers testing this technique could be gathered relatively easily by having them installing a simple app, this would not guarantee that they would gather in common areas.

Disclosure statement

No potential conflict of interest was reported by the authors.

Funding

This work was financially supported by JST-Mirai Program Grant Number JPMJMI17D4, JSPS KAKENHI Grant Number 25287026, the Doctoral Student Special Incentives Program (SEUT RA) and the Foundation for Supporting International Students of the University of Tokyo.

References

Abedi, Naeim, Ashish Bhaskar, Edward Chung, and Marc Miska. 2015. "Assessment of antenna characteristic effects on pedestrian and cyclists travel-time estimation based on Bluetooth and WiFi MAC addresses." *Transportation Research Part C: Emerging Technologies* 60: 124–141. https://doi.org/10.1016/j.trc.2015.08.010.

Boltes, Maik, Jette Schumann, and Daniel Salden. 2017. "Gathering of data under laboratory conditions for the deep analysis of pedestrian dynamics in crowds." In *Advanced Video and Signal Based Surveillance (AVSS), 2017 14th IEEE International Conference on*, 1–6. IEEE. https://doi.org/10.1109/AVSS.2017.8078471.

Boltes, Maik, and Armin Seyfried. 2013. "Collecting pedestrian trajectories." *Neurocomputing* 100: 127–133. https://doi.org/10.1016/j.neucom.2012.01.036.

Boltes, Maik, Armin Seyfried, Bernhard Steffen, and Andreas Schadschneider. 2010. "Automatic extraction of pedestrian trajectories from video recordings." In *Pedestrian and Evacuation Dynamics 2008*, 43–54. Springer. https://doi.org/10.1007/978-3-642-04504-2_3.

Brscic, Drazen, Takayuki Kanda, Tetsushi Ikeda, and Takahiro Miyashita. 2013. "Person tracking in large public spaces using 3-D range sensors." *IEEE Transactions on Human-Machine Systems* 43 (6): 522–534. https://doi.org/10.1109/THMS.2013.2283945.

Cao, Shuchao, Jun Zhang, Daniel Salden, Jian Ma, Chang'an Shi, and Ruifang Zhang. 2016. "Pedestrian dynamics in single-file movement of crowd with different age compositions." *Physical Review E* 94 (1): 012312. https://doi.org/10.1103/PhysRevE.94.012312.

Chattaraj, Ujjal, Armin Seyfried, and Partha Chakroborty. 2009. "Comparison of pedestrian fundamental diagram across cultures." *Advances in complex systems* 12 (03): 393–405. https://doi.org/10.1142/S0219525909002209.

Concone, Federico, Salvatore Gaglio, Giuseppe Lo Re, and Marco Morana. 2017. "Smartphone Data Analysis for Human Activity Recognition." In *AI*IA 2017 Advances in Artificial Intelligence: XVIth International Conference of the Italian Association for Artificial Intelligence*, 58–71. Springer International Publishing. https://doi.org/10.1007/978-3-319-70169-1_5.

Corbetta, Alessandro, Jasper Meeusen, Chung-min Lee, and Federico Toschi. 2016. "Continuous measurements of real-life bidirectional pedestrian flows on a wide walkway." In *Proceedings of Pedestrian and Evacuation Dynamics 2016*, 18–24. University of Science and Technology of China Press. https://doi.org/10.17815/CD.2016.11.

Daamen, Winnie, Yufei Yuan, and Dorine Duives. 2016. "Comparing three types of real-time data collection techniques: counting cameras, Wi-Fi sensors and GPS trackers." In *Proceedings of Pedestrian and Evacuation Dynamics 2016*, 568–574. University of Science and Technology of China Press. https://doi.org/10.17815/CD.2016.11.

Desa, UN. 2014. "World urbanization prospects, the 2014 revision." *United Nations* 366.

Feliciani, Claudio, and Katsuhiro Nishinari. 2016. "Pedestrians rotation measurement in bidirectional streams." In *Proceedings of Pedestrian and Evacuation Dynamics 2016*, 76–83. University of Science and Technology of China Press. https://doi.org/10.17815/CD.2016.11.

Feliciani, Claudio, and Katsuhiro Nishinari. 2018. "Measurement of congestion and intrinsic risk in pedestrian crowds." *Transportation Research Part C: Emerging Technologies* 91: 124–155. https://doi.org/10.1016/j.trc.2018.03.027.

Feliciani, Claudio, Francesco Zanlungo, Katsuhiro Nishinari, and Takayuki Kanda. 2019. "Thermodynamics of a gas of pedestrians: theory and experiment." In *Proceedings of Pedestrian and Evacuation Dynamics 2018*, Springer.

Feliz Alonso, Raúl, Eduardo Zalama Casanova, and Jaime Gómez García-Bermejo. 2009. "Pedestrian tracking using inertial sensors." https://doi.org/10.14198/JoPha.2009.3.1.05.

Glas, Dylan F, Takahiro Miyashita, Hiroshi Ishiguro, and Norihiro Hagita. 2009. "Laser-based tracking of human position and orientation using parametric shape modeling." *Advanced robotics* 23 (4): 405–428. http://dx.doi.org/10.1163/156855309X408754.

Gorrini, Andrea, Luca Crociani, Claudio Feliciani, Pengfei Zhao, Katsuhiro Nishinari, and Stefania Bandini. 2016. "Social Groups and Pedestrian Crowds: Experiment on Dyads in a Counter Flow Scenario." In *Proceedings of Pedestrian and Evacua-*

tion Dynamics 2016, 179–184. University of Science and Technology of China Press. https://doi.org/10.17815/CD.2016.11.

Hankin, BD, and Richard A Wright. 1958. "Passenger flow in subways." *Journal of the Operational Research Society* 9 (2): 81–88. https://doi.org/10.1057/jors.1958.9.

Helbing, Dirk, Anders Johansson, and Habib Zein Al-Abideen. 2007. "Dynamics of crowd disasters: An empirical study." *Physical review E* 75 (4): 046109. https://doi.org/10.1103/PhysRevE.75.046109.

Helbing, Dirk, and Pratik Mukerji. 2012. "Crowd disasters as systemic failures: analysis of the Love Parade disaster." *EPJ Data Science* 1 (1): 7. https://doi.org/10.1140/epjds7.

Höflinger, Fabian, Rui Zhang, and Leonhard M Reindl. 2012. "Indoor-localization system using a micro-inertial measurement unit (IMU)." In *European Frequency and Time Forum (EFTF), 2012*, 443–447. IEEE. https://doi.org/10.1109/EFTF.2012.6502421.

Hoogendoorn, Serge P, Winnie Daamen, and Piet HL Bovy. 2003. "Extracting microscopic pedestrian characteristics from video data." In *Transportation Research Board Annual Meeting*, 1–15.

Illiyas, Faisel T, Shibu K Mani, AP Pradeepkumar, and Keshav Mohan. 2013. "Human stampedes during religious festivals: A comparative review of mass gathering emergencies in India." *International Journal of Disaster Risk Reduction* 5: 10–18. https://doi.org/10.1016/j.ijdrr.2013.09.003.

Johansson, Anders, Dirk Helbing, Habib Z Al-Abideen, and Salim Al-Bosta. 2008. "From crowd dynamics to crowd safety: a video-based analysis." *Advances in Complex Systems* 11 (04): 497–527. https://doi.org/10.1142/S0219525908001854.

Junior, Julio Cezar Silveira Jacques, Soraia Raupp Musse, and Claudio Rosito Jung. 2010. "Crowd analysis using computer vision techniques." *IEEE Signal Processing Magazine* 27 (5): 66–77. https://doi.org/10.1109/MSP.2010.937394.

Karamouzas, Ioannis, Brian Skinner, and Stephen J Guy. 2014. "Universal power law governing pedestrian interactions." *Physical review letters* 113 (23): 238701. https://doi.org/10.1103/PhysRevLett.113.238701.

Kok, Ven Jyn, Mei Kuan Lim, and Chee Seng Chan. 2016. "Crowd behavior analysis: A review where physics meets biology." *Neurocomputing* 177: 342–362. https://doi.org/10.1016/j.neucom.2015.11.021.

Lara, Oscar D, and Miguel A Labrador. 2013. "A survey on human activity recognition using wearable sensors." *IEEE Communications Surveys and Tutorials* 15 (3): 1192–1209. https://doi.org/10.1109/SURV.2012.110112.00192.

Lin, Tao, Lingran Li, and Gérard Lachapelle. 2015. "Multiple sensors integration for pedestrian indoor navigation." In *Indoor Positioning and Indoor Navigation (IPIN), 2015 International Conference on*, 1–9. IEEE. https://doi.org/10.1109/IPIN.2015.7346785.

Lohner, Rainald, Britto Muhamad, Prabhu Dambalmath, and Eberhard Haug. 2018. "Fundamental Diagrams for Specific Very High Density Crowds." *Collective Dynamics* 2: 1–15. https://doi.org/10.17815/CD.2017.13.

Ministry of Land, Infrastructure, Transport and Tourism – Housing Bureau, Building Research Institute, Japan Conference of Building Officials, and The Building Center of Japan. 2001. *Explanation of the validation method for evacuation safety and calculation examples.* Inoueshoin. In Japanese.

Mohammadi, Sadegh, Hamed K Galoogahi, Alessandro Perina, and Vittorio Murino. 2017. "Physics-Inspired Models for Detecting Abnormal Behaviors in Crowded Scenes." *Group and Crowd Behavior for Computer Vision* 253. https://doi.org/10.1016/B978-0-12-809276-7.00013-8.

Mori, Kazuya, Akinori Yamane, Youhei Hayakawa, Tomotaka Wada, Kazuhiro Ohtsuki, and Hiromi Okada. 2013. "Development of emergency rescue evacuation support system (ERESS) in panic-type disasters: disaster recognition algorithm by support vector machine." *IEICE Transactions on Fundamentals of Electronics, Communications and Computer Sciences* 96 (2): 649–657. https://doi.org/10.1587/transfun.E96.A.649.

Mōri, Masamitsu, and Hiroshi Tsukaguchi. 1987. "A new method for evaluation of level of

service in pedestrian facilities." *Transportation Research Part A: General* 21 (3): 223–234. https://doi.org/10.1016/0191-2607(87)90016-1.

Nagao, Koki, Daichi Yanagisawa, and Katsuhiro Nishinari. 2018. "Estimation of crowd density applying wavelet transform and machine learning." *Physica A: Statistical Mechanics and its Applications* 510: 145–163. https://doi.org/10.1016/j.physa.2018.06.078.

Navin, Francis P, and Robert J Wheeler. 1969. "Pedestrian flow characteristics." *Traffic Engineering, Inst Traffic Engr* 39.

Oeding, Detlef. 1963. "Verkehrsbelastung und Dimensionierung von Gehwegen und anderen Anlagen des Fußgängerverkehrs." *Technische Hochschule Braunschweig Institut fur Stadtbauwesen, Dipl.-Ing., Strassenbau und Strassenverkehrstechnik* In German.

Older, SJ. 1968. "Movement of pedestrians on footways in shopping streets." *Traffic engineering & control* 10 (4).

Poapst, Rob. 2015. "Characterizing pedestrian traffic by hour-of-day periodicities in commercial zones." Master's thesis, University of Manitoba.

Seer, Stefan, Norbert Brändle, and Carlo Ratti. 2014. "Kinects and human kinetics: A new approach for studying pedestrian behavior." *Transportation research part C: emerging technologies* 48: 212–228. https://doi.org/10.1016/j.trc.2014.08.012.

Sekimoto, Yoshihide, Akihito Sudo, Takehiro Kashiyama, Toshikazu Seto, Hideki Hayashi, Akinori Asahara, Hiroki Ishizuka, and Satoshi Nishiyama. 2016. "Real-time people movement estimation in large disasters from several kinds of mobile phone data." In *Proceedings of the 2016 ACM International Joint Conference on Pervasive and Ubiquitous Computing: Adjunct*, 1426–1434. ACM. https://doi.org/10.1145/2968219.2968421.

Shimura, Kenichiro, Kazumichi Ohtsuka, Giuseppe Vizzari, Katsuhiro Nishinari, and Stefania Bandini. 2014. "Mobility analysis of the aged pedestrians by experiment and simulation." *Pattern Recognition Letters* 44: 58–63. https://doi.org/10.1016/j.patrec.2013.10.027.

Steffen, Bernhard, and Armin Seyfried. 2010. "Methods for measuring pedestrian density, flow, speed and direction with minimal scatter." *Physica A: Statistical mechanics and its applications* 389 (9): 1902–1910. https://doi.org/10.1016/j.physa.2009.12.015.

Stojanović, Dragan, and Natalija Stojanović. 2014. "Indoor localization and tracking: Methods, technologies and research challenges." *Facta Universitatis, Series: Automatic Control and Robotics* 13 (1): 57–72.

Su, Xing, Hanghang Tong, and Ping Ji. 2014. "Activity recognition with smartphone sensors." *Tsinghua Science and Technology* 19 (3): 235–249. https://doi.org/10.1109/TST.2014.6838194.

Transportation Research Board. 2010. *Highway Capacity Manual*. Transportation Research Board, National Research Council, Washington, DC.

Wąs, Jarosław, Jakub Porzycki, Robert Lubaś, Janusz Miller, and Grzegorz Bazior. 2015. "Agent based approach and Cellular Automata - A promising perspective in crowd dynamics modeling?" In *2015 Summer Solstice: 7th International Conference on Discrete Models of Complex Systems*, .

Weidmann, Ulrich. 1993. *Transporttechnik der Fussgänger: Transporttechnische Eigenschaften des Fussgängerverkehrs (Literaturauswertung)*. ETH, IVT. In German, https://doi.org/10.3929/ethz-a-000687810.

Yamamoto, Hiroki, Daichi Yanagisawa, Claudio Feliciani, and Katsuhiro Nishinari. 2017. "Modeling body-rotation behavior of pedestrians for collision avoidance in a narrow corridor." Submitted; January 2017.

Yanagisawa, Daichi, Hiroki Yamamoto, Takahiro Ezaki, and Katsuhiro Nishinari. 2016. "Passing in a narrow corridor: Modeling body rotation by ellipse." In *Proceedings of Pedestrian and Evacuation Dynamics 2016*, 213–220. University of Science and Technology of China Press. https://doi.org/10.17815/CD.2016.11.

Zhang, XL, WG Weng, and HY Yuan. 2012. "Empirical study of crowd behavior during a real mass event." *Journal of Statistical Mechanics: Theory and Experiment* 2012 (08): P08012. https://doi.org/10.1088/1742-5468/2012/08/P08012.

Zheng, Xiaoping, Tingkuan Zhong, and Mengting Liu. 2009. "Modeling crowd evacuation of

a building based on seven methodological approaches." *Building and Environment* 44 (3): 437–445. https://doi.org/10.1016/j.buildenv.2008.04.002.